

Whole Earth Geophysics

An Introductory Textbook for
Geologists and Geophysicists

Robert J. Lillie
Oregon State University

**GEOLOGY LIBRARY
SG GUYOT HALL
PRINCETON UNIVERSITY**



Prentice Hall
Upper Saddle River, New Jersey 07458

Library of Congress Cataloging-in-Publication Data

Lillie, Robert J.

Whole earth geophysics : an introductory textbook for geologists
and geophysicists / Robert J. Lillie

p. cm.

Includes bibliographical references and index.

ISBN 0-13-490517-2

1. Geophysics I. Title.

QC806.L48 1999

550—dc21

97-42092

CIP

*To my parents and grandmother,
for their inspiration and example.
To my son, Ben,
for his inspiration and example.
The Earth is a circle.*

Executive Editor: Robert A. McConnin

Art Director: Jayne Conte

Cover Designer: Bruce Kenselaar

Manufacturing Manager: Trudy Pisciotti

Production Supervision/Composition: WestWords, Inc.

Cover Illustration: Robert J. Lillie

Inside Cover Maps: A. Jon Kimerling

Text Illustrations: Robert J. Lillie



© 1999 by Prentice-Hall, Inc.
Simon & Schuster/A Viacom Company
Upper Saddle River, New Jersey 07458

All rights reserved. No part of this book may be
reproduced, in any form or by any means,
without permission in writing from the publisher.

Printed in the United States of America

10 9 8 7 6 5 4 3 2 1

ISBN 0-13-490517-2

(S)

R.C. B. 66

1/98

1/99

Prentice-Hall International (UK) Limited, *London*

Prentice-Hall of Australia Pty. Limited, *Sydney*

Prentice-Hall Canada Inc., *Toronto*

Prentice-Hall Hispanoamericana, S.A., *Mexico*

Prentice-Hall of India Private Limited, *New Delhi*

Prentice-Hall of Japan, Inc., *Tokyo*

Simon & Schuster Asia Pte. Ltd., *Singapore*

Editora Prentice-Hall do Brasil, Ltda., *Rio de Janeiro*

CHAPTER 8

Gravity and Isostasy

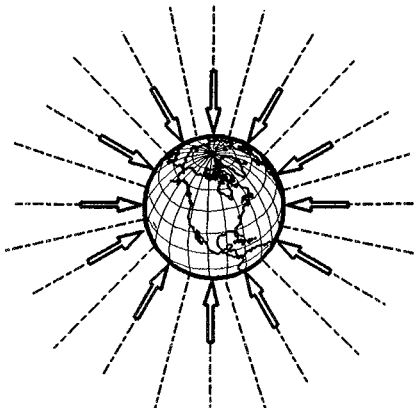
gravity (*grav' ə tē*) *n.*, [*< L. gravis, heavy*], 1. the force of attraction between masses 2. the force that tends to draw bodies in Earth's sphere toward Earth's center.

isostasy (*ī sā stā' sē*) *n.*, [*< Gr. isos, equal; < Gr. stasis, standing*], a state of balance whereby columns of material exert equal pressure at and below a compensating depth.

gravity and isostasy (*grav' ə tē ənd ī sā stā' sē*) *n.*, the study of spatial variations in Earth's gravitational field and their relationship to the distribution of mass within the Earth.

Earth's *gravity* and *magnetic forces* are potential fields that provide information on the nature of materials within the Earth. Potential fields are those in which the strength and direction of the field depend on the position of observation within the field; the strength of a potential field decreases with distance from the source. Compared to the magnetic field, Earth's gravity field is simple. Lines of force for the gravity field are directed toward the center of the Earth, while magnetic field strength and direction depend on Earth's positive and negative poles (Fig. 8.1).

a) *Gravity Field*



b) *Magnetic Field*

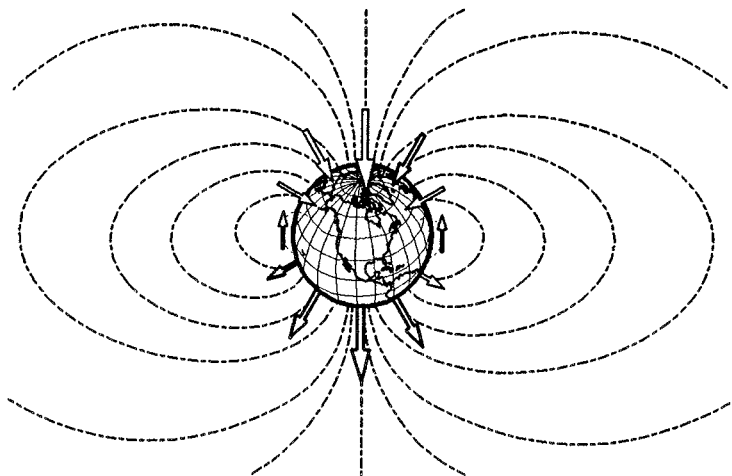


FIGURE 8.1 *Earth's potential fields.* a) The gravity field is symmetric. Force vectors (arrows) have approximately equal magnitude and point toward the center of the Earth. b) The magnitude and direction of the magnetic field is governed by positive (south) and negative (north) poles. Magnitude varies by a factor of two from equator to pole.

EARTH'S GRAVITY FIELD

Gravity is the attraction on one body due to the mass of another body. The force of one body acting on another is given by *Newton's Law of Gravitation* (Fig. 8.2a):

$$F = G \frac{m_1 m_2}{r^2}$$

where:

- F = force of attraction between the two objects (N)
- G = Universal Gravitational Constant ($6.67 \times 10^{-11} \text{ Nm}^2/\text{kg}^2$)
- m_1, m_2 = mass of the two objects (kg)
- r = distance between the centers of mass of the objects (m).

The force (F) exerted on the object with mass m_1 by the body with mass m_2 , is given by *Newton's Second Law of Motion* (Fig. 8.2b):

$$F = m_1 a$$

where:

- a = acceleration of object of mass m_1 due to the gravitational attraction of the object with mass m_2 (m/s^2).

Solving for the acceleration, then combining the two equations (Fig. 8.2c):

$$\begin{aligned} a &= \frac{F}{m_1} = \frac{1}{m_1} \frac{G m_1 m_2}{r^2} \\ a &= \frac{G m_2}{r^2} \end{aligned}$$

For Earth's gravity field (Fig. 8.3a), let:

g = \frac{GM}{R^2}

- a = g = gravitational acceleration observed on or above Earth's surface;
- m_2 = M = mass of the Earth;
- r = R = distance from the observation point to Earth's center of mass;

so that:

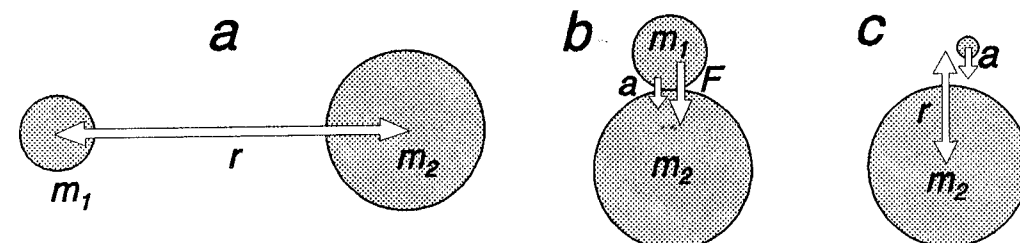


FIGURE 8.2 a) The gravitational force between two objects is directly proportional to their masses (m_1, m_2), and inversely proportional to the square of their distance (r). b) The mass (m_1), times the acceleration (a) due to mass (m_2), determines the gravitational force (F). c) The acceleration due to gravity (a) of a body depends only on the mass of the attracting body (m_2) and the distance to the center of that mass (r).

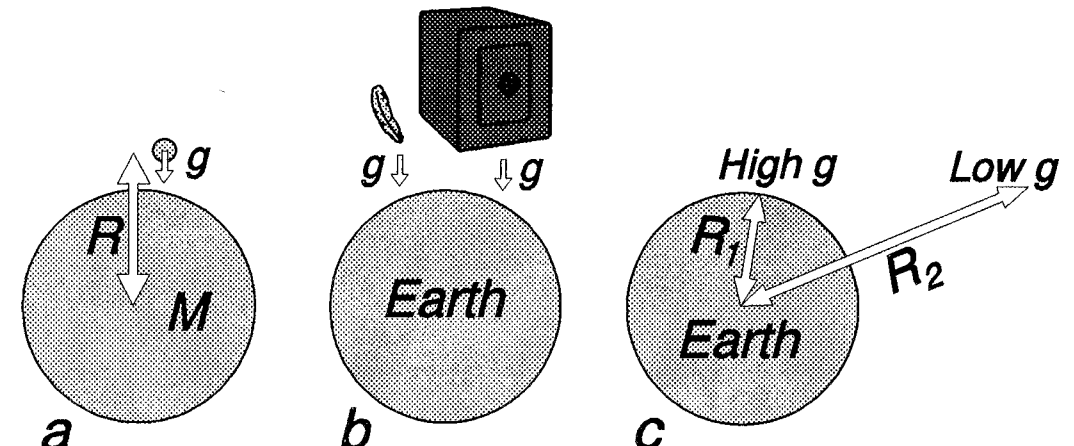


FIGURE 8.3 a) The mass (M) of the Earth and radius (R) to Earth's center determine the gravitational acceleration (g) of objects at and above Earth's surface. b) The acceleration is the same (g), regardless of the mass of the object. c) Objects at Earth's surface (radius R_1) have greater acceleration than objects some distance above the surface (radius R_2).

The above equation illustrates two fundamental properties of gravity. 1) Acceleration due to gravity (g) does *not* depend on the mass (m_1) attracted to the Earth (Fig. 8.3b); in the absence of air resistance, a small mass (feather) will accelerate toward Earth's surface at the same rate as a large mass (stone). 2) The farther from Earth's center of mass (that is, the greater the R), the smaller the gravitational acceleration (Fig. 8.3c); as a potential field, gravity thus obeys an *inverse square law*.

The value of the gravitational acceleration on Earth's surface varies from about 9.78 m/s^2 at the equator to about 9.83 m/s^2 at the poles (Fig. 8.4a). The smaller acceleration at the equator, compared to the poles, is because of the combination of three factors. 1) There is *less* inward acceleration because of *outward acceleration* caused by the spin of the Earth; the spin (rotation) is greatest at the equator but reduces to zero at the poles. 2) There is *less* acceleration at the equator because of the Earth's outward bulging, thereby increasing the radius (R) to the center of mass. 3) The added mass of the bulge creates *more* acceleration. Notice that the first two factors lessen the acceleration at the equator, while the third increases it. The net effect is the observed -0.05 m/s^2 difference.

Gravitational acceleration (gravity) is commonly expressed in units of *milligals* (mGal), where:

$$1 \text{ Gal} = 1 \text{ cm/s}^2 = 0.01 \text{ m/s}^2$$

so that:

$$1 \text{ mGal} = 10^{-3} \text{ Gal} = 10^{-3} \text{ cm/s}^2 = 10^{-5} \text{ m/s}^2.$$

Gravity, therefore, varies by about 5000 mGal from equator to pole (Fig. 8.4b).

GRAVITY ANOMALIES

Gravity observations can be used to interpret changes in mass below different regions of the Earth. To see the mass differences, the broad changes in gravity from equator to pole must be subtracted from station observations. This is accomplished

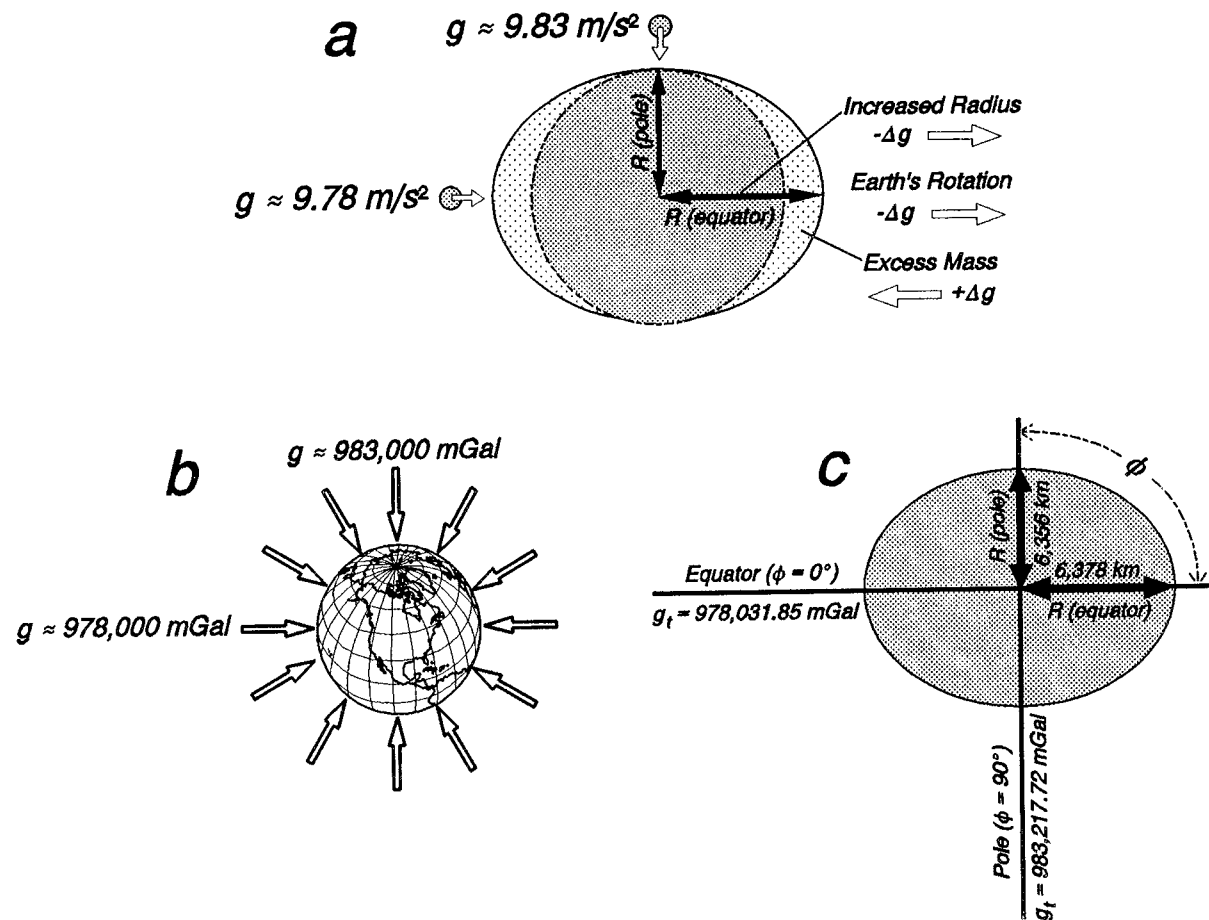


FIGURE 8.4 a) Three main factors responsible for the difference in gravitational acceleration at the equator compared to the poles. b) Gravity increases from about 978,000 mGal at the equator, to about 983,000 mGal at the poles. c) Variation in gravity from equator to pole, according to 1967 Reference Gravity Formula.

by predicting the gravity value for a station's latitude (*theoretical gravity*), then subtracting that value from the actual value at the station (*observed gravity*), yielding a *gravity anomaly*.

Theoretical Gravity

The average value of gravity for a given latitude is approximated by the 1967 *Reference Gravity Formula*, adopted by the International Association of Geodesy:

$$g_t = g_e (1 + 0.005278895 \sin^2 \phi + 0.000023462 \sin^4 \phi)$$

where:

- g_t = theoretical gravity for the latitude of the observation point (mGal)
- g_e = theoretical gravity at the equator (978,031.85 mGal)
- ϕ = latitude of the observation point (degrees).

The equation takes into account the fact that the Earth is an imperfect sphere, bulging out at the equator and rotating about an axis through the poles (Fig. 8.4a).

For such an *oblate spheroid* (Fig. 8.4c), it estimates that gravitational acceleration at the equator ($\phi = 0^\circ$) would be 978,031.85 mGal, gradually increasing with latitude to 983,217.72 mGal at the poles ($\phi = 90^\circ$).

Free Air Gravity Anomaly

Gravity observed at a specific location on Earth's surface can be viewed as a function of three main components (Fig. 8.5): 1) the *latitude* (ϕ) of the observation point, accounted for by the theoretical gravity formula; 2) the *elevation* (ΔR) of the station, which changes the radius (R) from the observation point to the center of the Earth; and 3) the *mass distribution* (M) in the subsurface, relative to the observation point.

The *free air correction* accounts for the second effect, the local change in gravity due to elevation. That deviation can be approximated by considering how gravity changes as a function of increasing distance of the observation point from the center of mass of the Earth (Fig. 8.4a). Consider the equation for the gravitational acceleration (g) as a function of radius (R):

$$g = \frac{GM}{R^2}$$

The first derivative of g , with respect to R , gives the change in gravity (Δg) with increasing distance from the center of the Earth (that is, increasing elevation, ΔR):

$$\lim_{\Delta R \rightarrow 0} \frac{\Delta g}{\Delta R} = \frac{dg}{dR} = -2 \left(\frac{GM}{R^3} \right) = -2 \left(\frac{GM}{R^2} \right) = -\frac{2g}{R}$$

$$\frac{dg}{dR} = -\frac{2g}{R}$$

Assuming average values of $g \approx 980,625 \text{ mGal}$ and $R \approx 6,367 \text{ km} = 6,367,000 \text{ m}$ (Fig. 8.4c):

$$dg/dR \approx -0.308 \text{ mGal/m}$$

where:

dg/dR = average value for the change in gravity with increasing elevation.

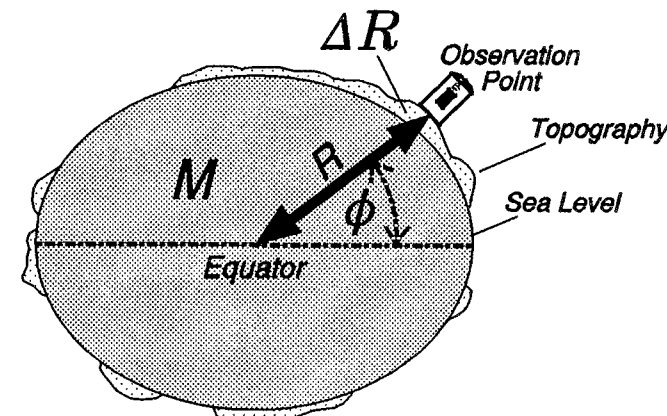


FIGURE 8.5 Three factors determining gravity at an observation point: a) latitude (ϕ); b) distance from sea-level datum to observation point (ΔR); c) Earth's mass distribution (M), relative to the station location (M includes material above as well as below sea level). ϕ is accounted for by subtracting the theoretical gravity from the observed gravity, and ΔR by the free air correction. The remaining value (free air anomaly) is thus a function of M .

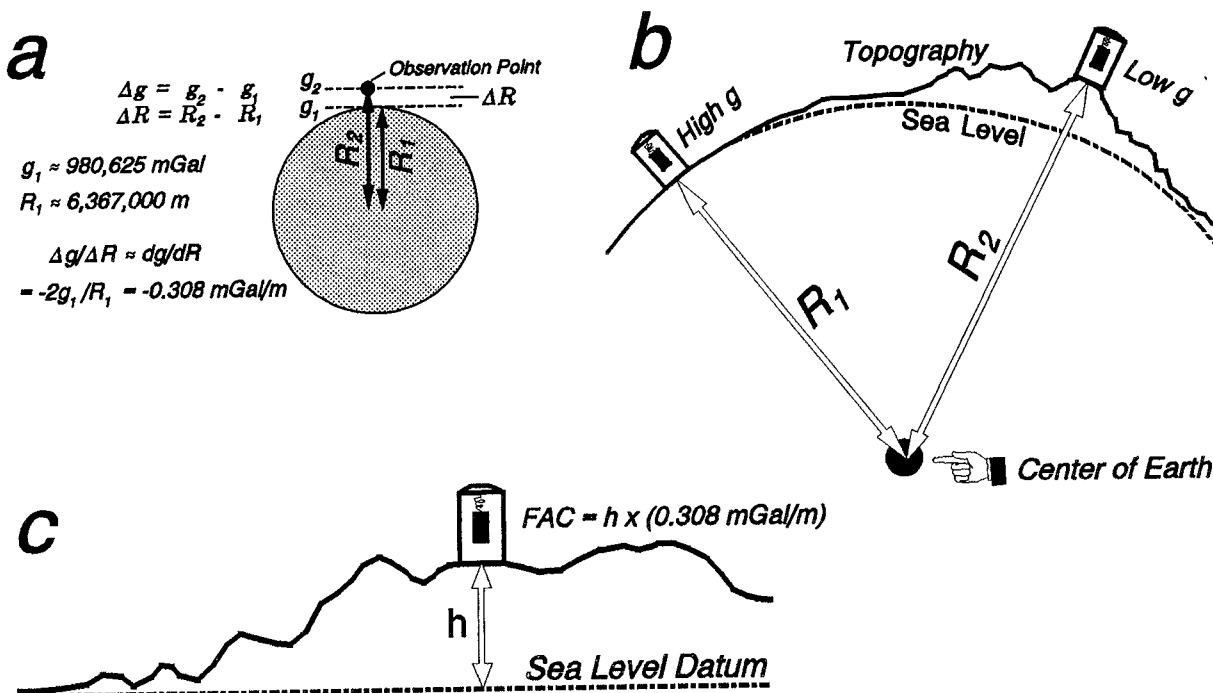


FIGURE 8.6 Free air correction. a) Rising upward from Earth's surface, gravitational acceleration decreases by about 0.308 mGal for every meter of height. b) A gravity station at high elevation tends to have a lower gravitational acceleration (g) than a station at lower elevation. c) The free air correction (FAC) accounts for the extended radius to an observation point, elevated h meters above a sea level datum.

The above equation illustrates that, for every 3 m (about 10 feet) upward from the surface of the Earth, the acceleration due to gravity decreases by about 1 mGal. Stations at elevations high above sea level therefore have lower gravity readings than those near sea level (Fig. 8.6b). To compare gravity observations for stations with different elevations, a *free air correction* must be added back to the observed values (Fig. 8.6c).

$$\text{FAC} = h \times (0.308 \text{ mGal/m})$$

where:

FAC = free air correction (mGal)

h = elevation of the station above a sea level datum (m).

The *free air gravity anomaly* is the observed gravity, corrected for the latitude and elevation of the station:

$$\Delta g_{fa} = g - g_t + \text{FAC}$$

where:

Δg_{fa} = free air gravity anomaly

g = gravitational acceleration observed at the station.

Notice in the above equation that: 1) subtracting the theoretical gravity (g_t) from the observed gravity (g) corrects for the *latitude*, thus accounting for the spin and

bulge of the Earth; and 2) adding the free air correction (FAC) puts back the gravity lost to *elevation*, thereby correcting for the increased radius (R) to Earth's center.

The free air gravity anomaly is a function of *lateral mass variations* (M in Fig. 8.5), because the latitude and elevation effects (ϕ and ΔR in Fig. 8.5) have been corrected. Fig. 8.7 shows what a profile of changing free air anomalies might look like across bodies of excess and deficient mass. Notice that the anomaly shows relatively high readings near the mass excess, low readings near the mass deficiency; there are also abrupt changes that mimic sharp topographic features.

Bouguer Gravity Anomaly

Even after elevation corrections, gravity can vary from station to station because of differences in mass between the observation points and the sea-level datum. Relative to areas near sea level, mountainous areas would have extra mass, tending to increase the gravity (Fig. 8.8a).

The *Bouguer correction* accounts for the gravitational attraction of the mass above the sea-level datum. This is done by approximating the mass as an *infinite slab*, with thickness (h) equal to the elevation of the station (Fig. 8.8b). The attraction of such a slab is:

$$\text{BC} = 2\pi\rho Gh$$

where:

BC = Bouguer correction

ρ = density of the slab

G = Universal Gravitational Constant

h = thickness of the slab (station elevation).

Substituting the values of G and 2π yields:

$$\text{BC} = 0.0419\phi$$

where BC is in mGal (10^{-5} m/s^2); ρ in g/cm^3 (10^3 kg/m^3); h in m.

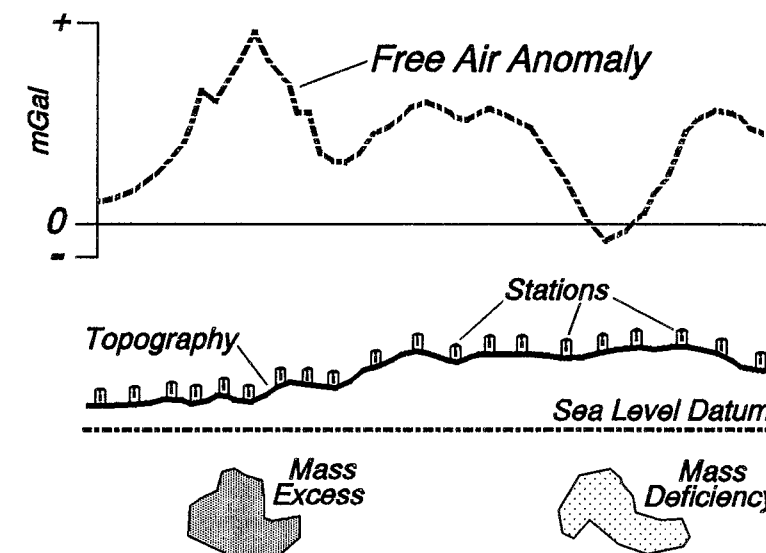


FIGURE 8.7 General form of free air gravity anomaly profile across areas of mass excess and mass deficiency.

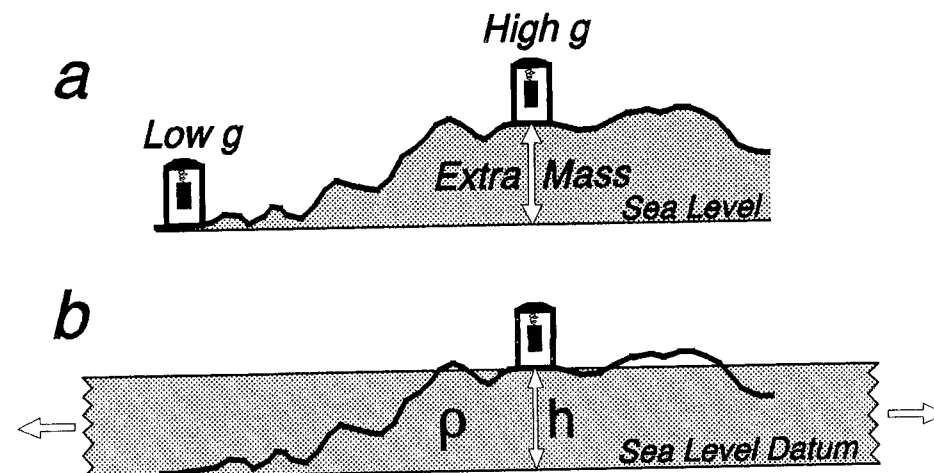


FIGURE 8.8 Bouguer correction. a) The extra mass of mountains results in higher gravity relative to areas near sea level. b) To account for the excess mass above a sea level datum, the Bouguer correction assumes an infinite slab of density (ρ), with thickness (h) equal to the station's elevation.

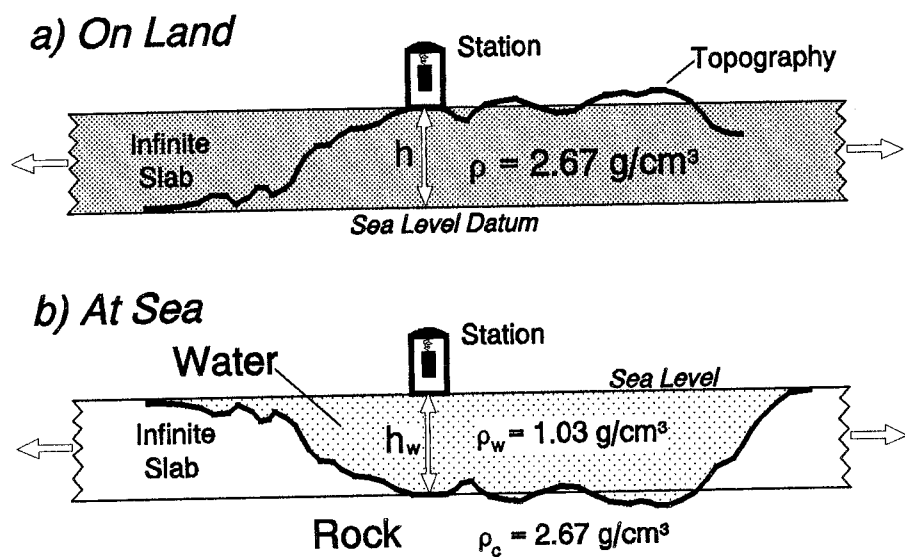


FIGURE 8.9 Standard Bouguer correction values. a) On land, the reduction density (ρ) is commonly taken as $+2.67 \text{ g/cm}^3$. The thickness of the infinite slab is equal to the station elevation (h). b) At sea, the reduction density (-1.64 g/cm^3) is the difference between that of sea water (1.03 g/cm^3) and underlying rock (2.67 g/cm^3). The thickness of the slab is equal to the water depth (h_w).

Bouguer Gravity Anomaly on Land For regions above sea level (Fig. 8.9a), the *simple Bouguer gravity anomaly* (Δg_B) results from subtracting the effect of the infinite slab (BC) from the free air gravity anomaly:

$$\Delta g_B = \Delta g_{fa} - BC$$

To determine the Bouguer correction, the density of the infinite slab (ρ) must be assumed (the *reduction density*). The reduction density is commonly taken as 2.67 g/cm^3 , a typical density of granite (Figs. 3.9, 3.10).

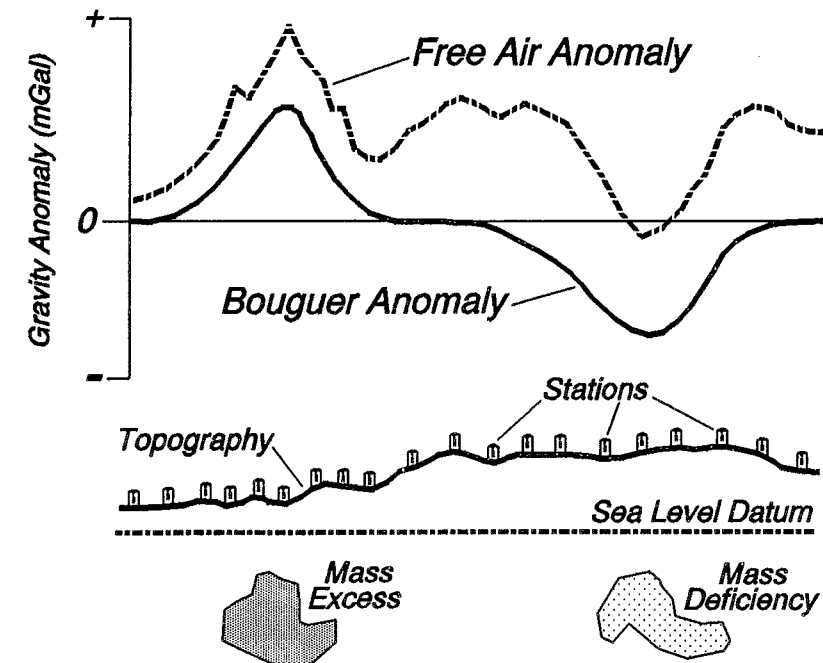


FIGURE 8.10 Bouguer correction applied to the free air gravity anomaly profile in Fig. 8.7.

The standard Bouguer correction for areas above sea level is thus:

$$\begin{aligned} BC &= 0.0419ph = (0.0419)(2.67\text{g/cm}^3)h \\ &= (0.112 \text{ mGal/m}) \times h \end{aligned}$$

where h is in m. The equation illustrates that, for about every 9 m of surface elevation, the increased mass below the observation point adds about 1 mGal to the observed gravity. Using the standard correction, the *simple Bouguer gravity anomaly on land* is computed from the free air gravity anomaly according to the formula:

$$\Delta g_B = \Delta g_{fa} - (0.112 \text{ mGal/m}) h$$

(h in meters).

Like the free air gravity anomaly, the Bouguer gravity anomaly reflects changes in mass distribution below the surface. The Bouguer anomaly, however, has had an additional correction, removing most of the effect of mass excess above a sea level datum (on land). Bouguer Corrections applied to the free air gravity profile (Fig. 8.7) would therefore yield a Bouguer gravity profile illustrated in Fig. 8.10. The two profiles illustrate three general properties of gravity anomalies. 1) For stations above sea level, the Bouguer anomaly is always less than the free air anomaly (the approximate attraction of the mass above sea level has been removed from the free air anomaly). 2) Short-wavelength changes in the free air anomaly, due to abrupt topographic changes, have been removed by the Bouguer correction; the Bouguer anomaly is therefore smoother than the free air anomaly. 3) Mass excesses result in positive changes in gravity anomalies; mass deficiencies cause negative changes.

Bouguer Gravity Anomaly at Sea In areas covered by the sea, gravity is generally measured on the surface of the water (Fig. 8.9b). In the strictest sense,

Bouguer anomalies at sea are exactly the same as free air anomalies, because station elevations (h) are zero:

$$\Delta g_B = \Delta g_{fa} - 0.0419ph; h = 0, \text{ so that: } \Delta g_B = \Delta g_{fa}$$

A type of Bouguer correction can be applied, however, because the density and depth of the water are well known. Instead of stripping the topographic mass away, as is done on land, the effect can be thought of as “pouring concrete” to fill the ocean. Thus, the Bouguer correction at sea can be envisioned as an infinite slab, equal to the depth of the water and with density equalling the difference between that of water and “concrete”:

$$BC_s = 0.0419ph = 0.0419(\rho_w - \rho_c)h_w$$

where:

BC_s = Bouguer correction at sea

ρ_w = density of sea water

ρ_c = density of “concrete”

h_w = water depth below the observation point.

Assuming $\rho_w = 1.03 \text{ g/cm}^3$ and $\rho_c = 2.67 \text{ g/cm}^3$:

$$BC_s = 0.0419 (-1.64 \text{ g/cm}^3) h_w = -0.0687 (\text{mGal/m}) \times h_w$$

where BC_s is in mGal and h_w in m.

Retaining the convention defined above, the Bouguer correction at sea is subtracted from the free air anomaly to yield the *Bouguer gravity anomaly at sea* (Δg_{Bs}):

$$\Delta g_{Bs} = \Delta g_{fa} - BC_s$$

Notice that the water is a mass deficit when compared to adjacent landmasses of rock; the negative Bouguer correction at sea thus means that some value must be added to the free air anomaly to compute the Bouguer anomaly at sea:

$$\Delta g_{Bs} = \Delta g_{fa} + (0.0687 \text{ mGal/m}) h_w \quad (h_w \text{ in meters}).$$

Complete Bouguer Gravity Anomaly The infinite slab correction described above yields a simple Bouguer anomaly. That correction is normally sufficient to approximate mass above the datum in the vicinity of the station (Fig. 8.11a). In rugged areas, however, there may be significant effects due to nearby mountains pulling upward on the station, or valleys that do not contain mass that was subtracted (Fig. 8.11b). For such stations, additional *terrain corrections* (TC; see Telford et al., 1976) are applied to the simple Bouguer anomaly (Δg_B), yielding the *complete Bouguer gravity anomaly* (Δg_{Bc}):

$$\Delta g_{Bc} = \Delta g_B + TC$$

Summary of Equations for Free Air and Bouguer Gravity Anomalies

Fig. 8.12 illustrates parameters used to determine free air and Bouguer gravity anomalies. The formulas below yield standard versions of the anomalies.

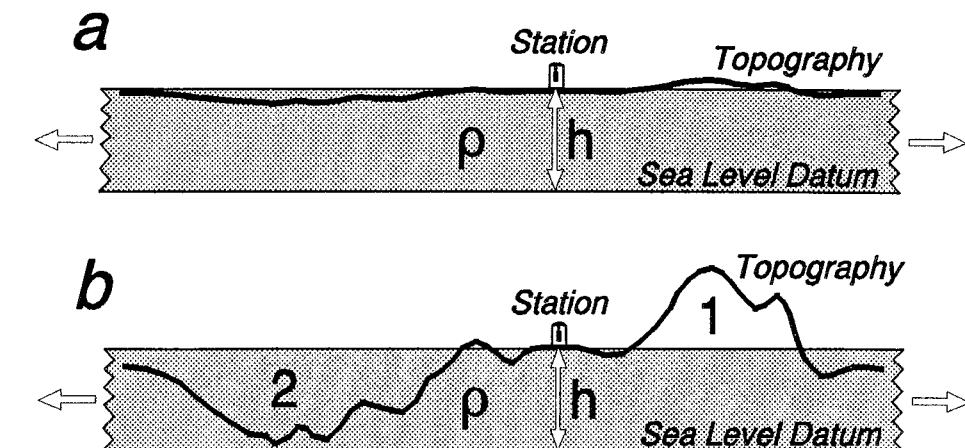


FIGURE 8.11 *Terrain correction.* a) In areas of low relief, the Bouguer slab approximation is adequate; terrain correction is unnecessary. b) High relief areas require terrain correction, to account for lessening of observed gravity due to mass of mountains above the slab (1), and overcorrection due to valleys (2). For both situations, the terrain correction is positive, making the complete Bouguer anomaly higher than the simple Bouguer anomaly.

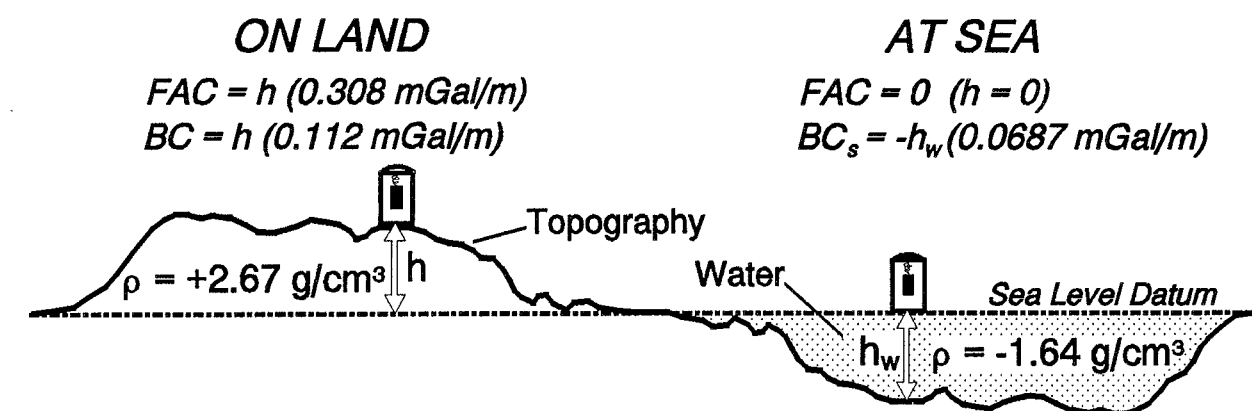


FIGURE 8.12 Standard parameters used to compute gravity anomalies on land and at sea. FAC = free air correction; BC = Bouguer correction; BC_s = Bouguer correction at sea; ρ = reduction density; h (elevation) and h_w (water depth) in meters.

Theoretical Gravity

$$g_t = g_e (1 + 0.005278895 \sin^2 \phi + 0.000023462 \sin^4 \phi)$$

g_t = theoretical gravity for the latitude of the observation point (mGal)
 g_e = theoretical gravity at the equator ($978,031.85 \text{ mGal}$)
 ϕ = latitude of the observation point (degrees).

Free Air Gravity Anomaly

$$\Delta g_{fa} = (g - g_e) + h(0.308 \text{ mGal/m})$$

Δg_{fa} = free air gravity anomaly (mGal)

g = observed gravity ($mGal$)
 g_t = theoretical gravity ($mGal$)
 h = elevation above sea level datum (m).

Bouguer Gravity Anomaly

$$\Delta g_B = \Delta g_{fa} - BC$$

$$= \Delta g_{fa} - 0.0419\rho h$$

BC = Bouguer correction ($mGal$)
 ρ = reduction density (g/cm^3)

a) On Land

$$\Delta g_B = \Delta g_{fa} - (0.112 \text{ mGal/m}) h \quad (\text{for } \rho = +2.67)$$

Δg_B = simple Bouguer gravity anomaly ($mGal$)
 h = elevation above sea-level datum (m).

b) At Sea

$$\Delta g_{Bs} = \Delta g_{fa} + (0.0687 \text{ mGal/m}) h_w \quad (\text{for } \rho = -1.64)$$

Δg_{Bs} = Bouguer gravity anomaly at sea ($mGal$)
 h_w = water depth below observation point (m).

c) In Rugged Terrain:

$$\Delta g_{Bc} = \Delta g_B + TC$$

Δg_{Bc} = complete Bouguer gravity anomaly ($mGal$)
 TC = terrain correction ($mGal$).

MEASUREMENT OF GRAVITY

Gravitational acceleration on Earth's surface can be measured in absolute and relative senses (Fig. 8.13). *Absolute gravity* reflects the actual acceleration of an object as it falls toward Earth's surface, while *relative gravity* is the difference in gravitational acceleration at one station compared to another.

a) Absolute Gravity

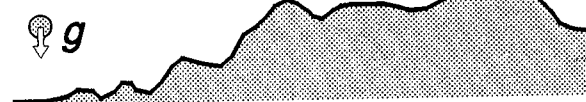
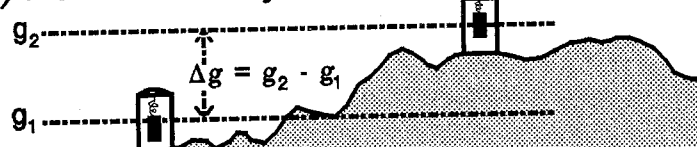
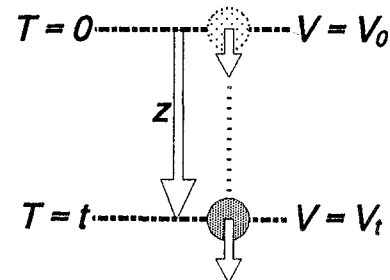


FIGURE 8.13 a) Absolute gravity is the true gravitational acceleration (g). b) Relative gravity reflects the difference in gravitational acceleration (Δg) at one station (g_1) compared to another (g_2).

b) Relative Gravity



a) Weight Drop



b) Pendulum

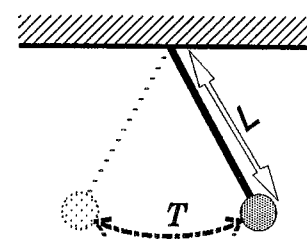


FIGURE 8.14 Measurement of absolute gravity. a) Weight drop. The object accelerates from an initial velocity of V_0 at time ($T = 0$), to a velocity of V_t at time ($T = t$), as it falls a distance (z). b) Pendulum. Gravitational acceleration is a function of the pendulum's length (L) and period of oscillation (T).

Absolute Gravity

There are two basic ways to measure absolute gravity. In the *weight drop* method (Fig. 8.14a), the velocity and displacement are measured for an object in free fall. The absolute gravity is computed according to:

$$z = v_0 t + \frac{1}{2} g t^2$$

where:

z = distance the object falls
 t = time to fall the distance z
 v_0 = initial velocity of the object
 g = absolute gravity.

The absolute gravity is thus:

$$g = 2(z - v_0 t)/t^2$$

Using the second method (Fig. 8.14b), a *pendulum* oscillates according to:

$$T = 2\pi\sqrt{L/g}$$

where:

T = period of swing of the pendulum
 L = length of the pendulum.

The absolute gravity is computed according to:

$$g = L(4\pi^2/T^2)$$

Relative Gravity

The precision necessary to obtain reliable, absolute gravity observations makes those measurements expensive and time consuming. Relative gravity measurements, however, can be done easily, with an instrument (*gravimeter*) that essentially measures the length of a spring (L ; Fig. 8.15a). The *mass* of an object suspended from the spring remains constant. When the gravimeter is taken from one station location to another, however, the *force* (F) that the mass (m) exerts on the spring varies with the local gravitational acceleration (g):

$$F = mg$$

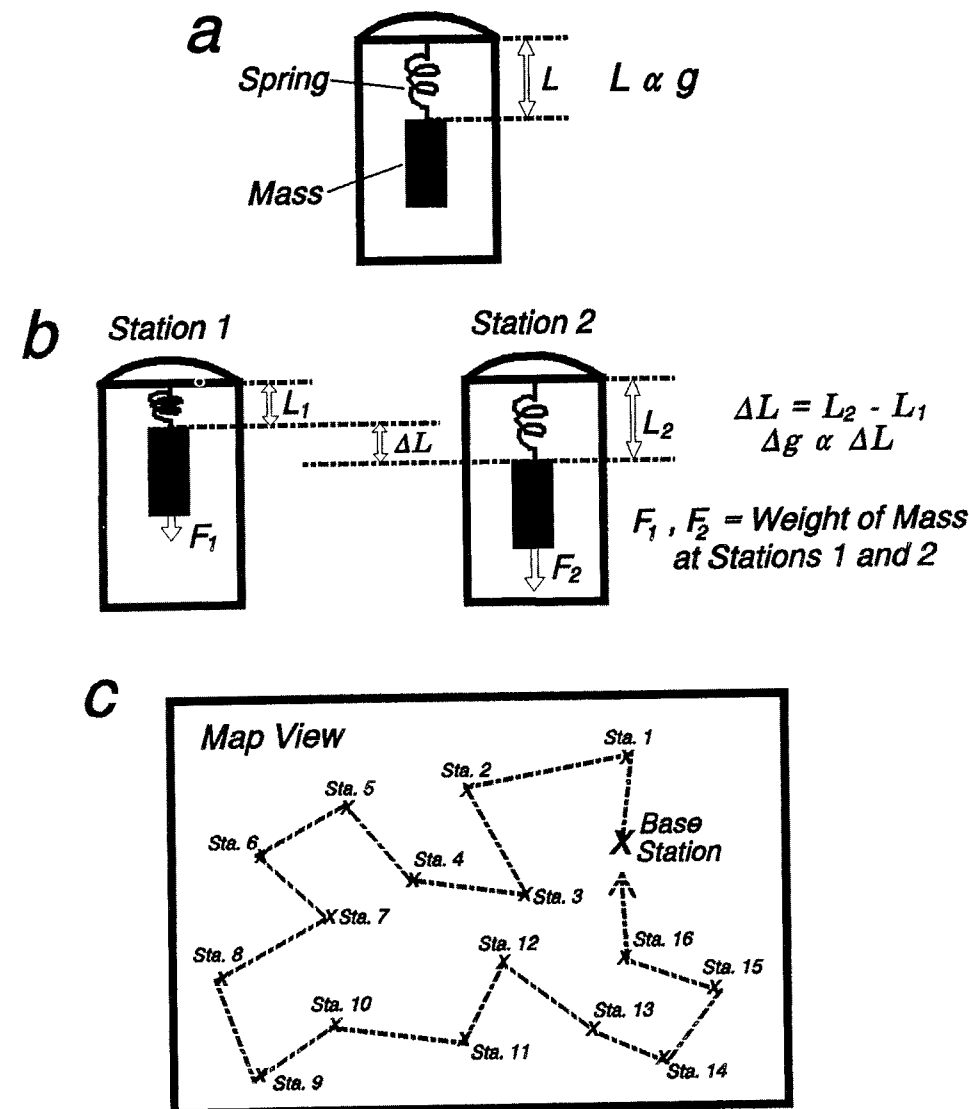


FIGURE 8.15 Measurement of relative gravity. a) A gravimeter measures the length of a spring (L), which is proportional to the gravitational acceleration (g). b) A force (F_1) at one station results in a spring length (L_1). The length may change to L_2 because of a different force (F_2) at another station. The force exerted by the mass is a function of g ; the change in length of the spring (ΔL) is thus proportional to the change in gravitational acceleration (Δg). c) Map of relative gravity survey. The traverse starts with a measurement at the base station, then each of the 16 stations, followed by a re-measurement at the base station.

so that:

$$g = F/m$$

In other words, the mass will weigh more or less (exert more or less force), depending on the pull of gravity (g) at the station. A gravimeter is simply weighing the mass at different stations; the spring stretches ($+ΔL$) where there is more gravity and contracts ($-ΔL$) when gravity is less (Fig. 8.15b).

If we know the absolute gravity at a starting point (base station), we can use a gravimeter to measure points relative to that station (Fig. 8.15c). The initial reading

(that is, the initial length of the spring) measured at the base station represents the absolute gravity at that point. Measurements are then taken at other stations, with the changes in length of the spring recorded. The gravimeter is calibrated so that a given change in spring length ($ΔL$) represents a change in gravity ($Δg$) by a certain amount (in mGal). The acceleration (g) can then be computed by adding the value of $Δg$ to the absolute gravity of the base station.

At sea, gravity surveying is complicated by the fact that the measurement platform is unstable. Waves move the ship up and down, causing accelerations that add or subtract from the gravity. Also, like Earth's rotation, the speed of the ship over the water results in an outward acceleration; in other words, the ship's velocity adds to the velocity of Earth's rotation. An additional correction, known as the *Eötvös correction*, is therefore added to marine gravity measurements (Telford et al., 1976):

$$\text{EC} = 7.503 V \cos\phi \sin\alpha + 0.004154 V^2$$

where:

EC = Eötvös correction (mGal)

V = speed of ship (knots; 1 knot = 1.852 km/hr = 0.5144 m/s)

φ = latitude of the observation point (degrees)

α = course direction of ship (azimuth, in degrees).

ISOSTASY

Until quite recently, surveyors leveled their instruments by suspending a lead weight (plumb bob) on a string. In the vicinity of large mountains, it was recognized that a correction must be made because the *mass excess* of the mountains standing high above the surveyor's location made the plumb bob deviate slightly from the vertical (Fig. 8.16a).

In the mid-1800's a large-scale survey of India was undertaken. Approaching the Himalaya Mountains from the plains to the south, the correction was calculated and applied. A systematic error was later recognized, however, as the plumb bob was not deviated toward the mountains as much as it should have been (Fig. 8.16b). This difference was attributed to *mass deficiency* within the Earth, beneath the excess mass of the mountains.

Pratt and Airy Models (Local Isostasy)

Scientists proposed two models to explain how the mass deficiency relates to the topography of the Himalayas. *Pratt* assumed that the crust of the Earth comprised blocks of different density; blocks of lower density need to extend farther into the air in order to exert the same pressure as thinner blocks of higher density (Fig. 8.17a). The situation is analogous to blocks of wood, each of different density, floating on water. By the Pratt model, the base of the crust is flat, so that the surface of equal pressure (depth of compensation) is essentially a flat crust/mantle boundary.

In the model of *Airy* (Fig. 8.17b), crustal blocks have equal density, but they float on higher-density material (Earth's mantle), similar to (low-density) icebergs floating on (higher-density) water. The base of the crust is thus an exaggerated, mirror image of the topography. Areas of high elevation have low-density "crustal roots" supporting their weight, much like a beach ball lifting part of a swimmer's body out of the water.

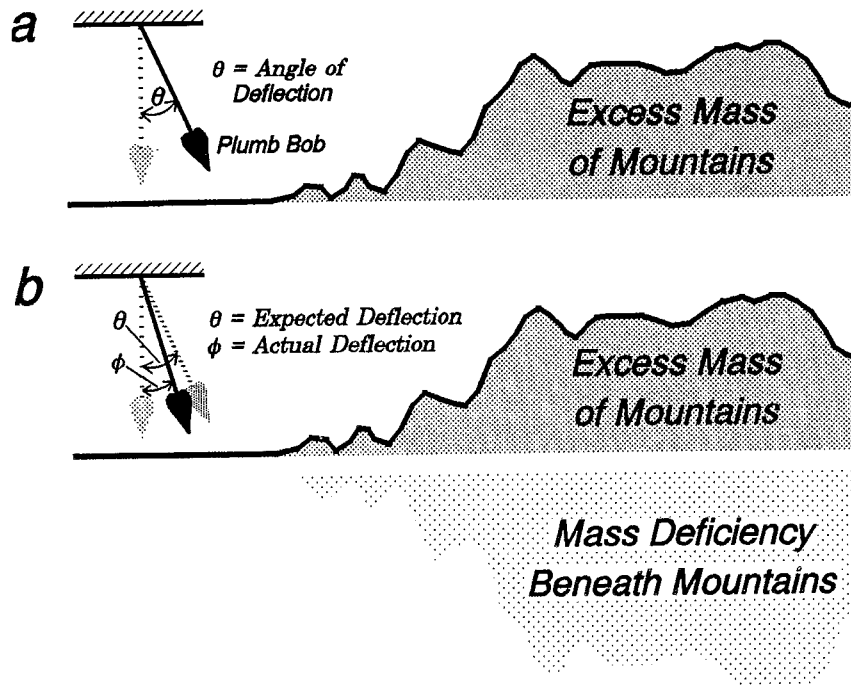


FIGURE 8.16 a) Expected deflection of a plumb bob (highly exaggerated), due to the attraction of the mass of a mountain range. b) The actual deflection for the Himalayas was less than expected, due to a deficiency of mass beneath the mountains.

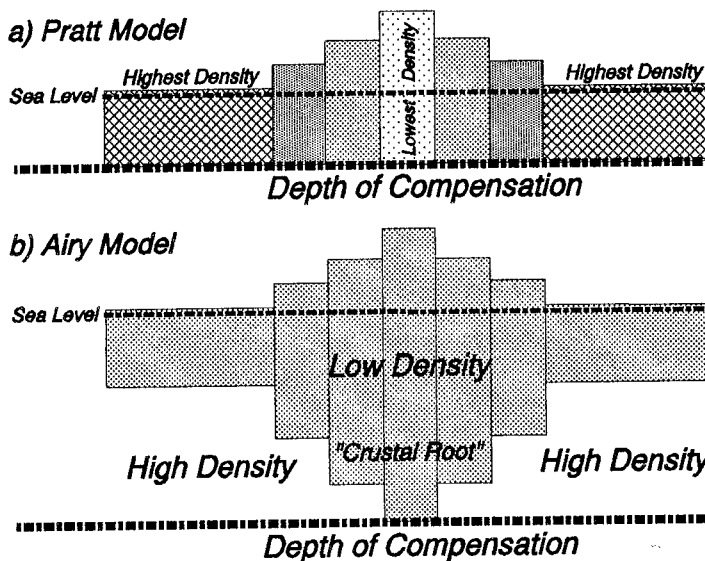


FIGURE 8.17 Pratt and Airy models of local isostatic compensation. In both models, pressure exerted by crustal columns is equal on horizontal planes at and below the depth of compensation.

Hydrostatic pressure is the pressure exerted on a point within a body of water. Similarly, pressure at a given depth within the Earth (Fig. 8.18a) can be viewed as lithostatic pressure, according to:

$$P = \rho g z$$

where:

P = pressure at the point within the Earth
 ρ = average density of the material above the point

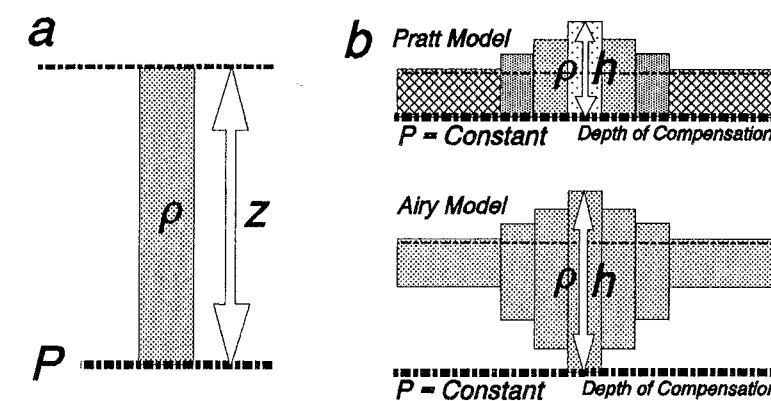


FIGURE 8.18 a) Pressure (P) at depth (z) is a function of the density (ρ) of the material above a point within the Earth. b) For the Pratt and Airy models, the pressure depends on the density and thickness (h) of crustal blocks. In both models, pressure equalizes at the depth of compensation.

$$g = \text{acceleration due to gravity} (\approx 9.8 \text{ m/s}^2)$$

$$z = \text{depth to the point.}$$

For the Pratt and Airy models (Fig. 8.18b), the pressure exerted by a crustal block can be expressed as:

$$P = \rho g h$$

where:

$$P = \text{pressure exerted by the crustal block}$$

$$\rho = \text{density of the crustal block}$$

$$h = \text{thickness of the crustal block.}$$

In both the Pratt and Airy models, the pressure must be the same everywhere at the *depth of compensation*. For the Pratt model, the base of each block is at the exact depth of compensation, so that:

$$P = \rho_2 h_2 = \rho_3 h_3 = \rho_4 h_4 = \rho_5 h_5$$

where:

$$\rho_2, \rho_3, \rho_4, \rho_5 = \text{density of each block}$$

$$h_2, h_3, h_4, h_5 = \text{thickness of each block.}$$

Dividing out a constant gravitational acceleration (g):

$$\boxed{P/g = \rho_2 h_2 = \rho_3 h_3 = \rho_4 h_4 = \rho_5 h_5}$$

In the particular Pratt model shown in Fig. 8.19a, $\rho_5 < \rho_4 < \rho_3 < \rho_2 < \rho_1$, where ρ_1 is the density of the substratum (Earth's mantle).

In an Airy model the crustal density (ρ_2) is constant and less than the mantle density (ρ_1). Only the thickest crustal block extends to the depth of compensation. For the Airy isostatic model in Fig. 8.19b, the pressure exerted at the depth of compensation (divided by g) is:

$$\boxed{P/g = \rho_2 h_5 = (\rho_2 h_4 + \rho_1 h'_4) = (\rho_2 h_3 + \rho_1 h'_3) = (\rho_2 h_2 + \rho_1 h'_2)}$$

where:

h'_2, h'_3, h'_4 = thickness of mantle column from the base of each crustal block to the depth of compensation.

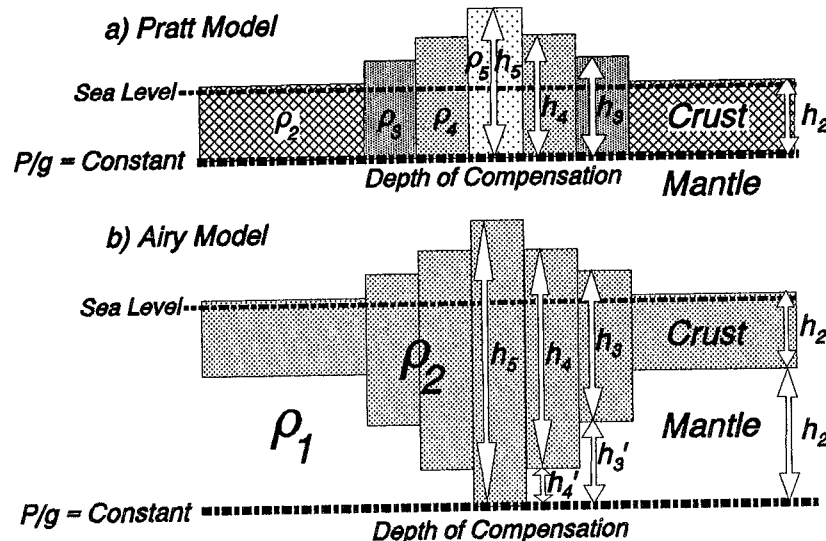


FIGURE 8.19 Density (ρ) and thickness (h, h') relationships for Pratt and Airy isostatic models. P = pressure; g = gravitational acceleration.

$$\frac{P}{g} = \rho_a h_a + \rho_w h_w + \rho_c h_c + \rho_m h_m = \text{Constant}$$

where:

- ρ_a = density of the air ($\rho_a \approx 0$)
- h_a = thickness of the air column, up to the level of the highest topography
- ρ_w = density of the water
- h_w = thickness of the water column
- ρ_c = density of the crust
- h_c = thickness of the crust
- ρ_m = density of the mantle
- h_m = thickness of the mantle column, down to the depth of compensation.

- 2) The total thickness (T) of each vertical column is constant:

$$T = h_a + h_w + h_c + h_m = \text{Constant}$$

If the isostatic column (P/g) can be determined or assumed for one area, then solving the two equations simultaneously can be used to estimate thicknesses (h) and/or densities (ρ) for vertical columns beneath other areas.

Airy Isostatic Model

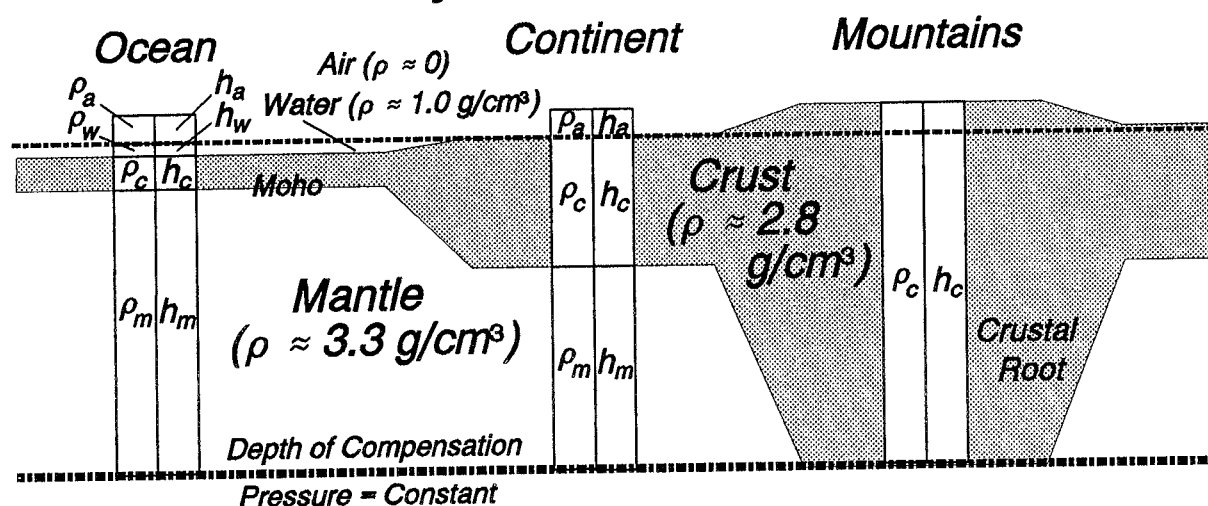


FIGURE 8.20 Airy isostatic model. Oceanic regions have thin crust, relative to continental regions. The weight of extra mantle material beneath the thin oceanic crust pulls downward until just enough depth of water fills the basin to achieve isostatic equilibrium. Mountainous regions have thick crust, relative to normal continental regions. The crustal root exerts an upward force until it is balanced by the appropriate weight of mountains.

While regions often exhibit components of both hypotheses, isostatic compensation is generally closer to the Airy than the Pratt model. Pure Airy isostatic compensation for regions with oceanic and continental crust, as well as thickened crust weighted down by mountains, might exhibit the form illustrated in Fig. 8.20. Notice that the crustal root beneath elevated regions is typically 5 to 8 times the height of the topographic relief. At the *depth of compensation* beneath each region, two equations hold true. 1) The total *pressure* (P) exerted by each vertical column, divided by the gravitational acceleration (g), is constant:

Lithospheric Flexure (Regional Isostasy)

Both the Pratt and Airy models assume *local isostasy*, whereby compensation occurs directly below a load (Fig. 8.21a); supporting materials behave like liquids, flowing to accommodate the load. In other words, the materials are assumed to have *no rigidity*. Most Earth materials, however, are somewhat rigid; the effect of a load is distributed over a broad area, depending on the *flexural rigidity* of the supporting material. Models of *regional isostasy* therefore take lithospheric strength into account (Fig. 8.21b).

A common model of regional isostatic compensation is that of an *elastic plate* that is bent by topographic and subsurface loads. The *flexural rigidity* (D) of the plate determines the degree to which the plate supports the load. The elastic plate model is analogous to a diving board, the *load* being the *diver* standing near the end of the board (Fig. 8.22). A thin, weak board (small D) bends greatly, especially near the diver. A thicker board of the same material behaves more rigidly; the diver causes a smaller deflection. The flexural rigidity (resistance to bending) thus depends on the *elastic thickness* of each board.

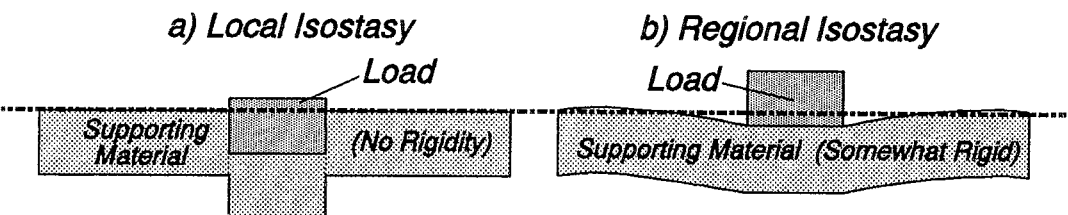


FIGURE 8.21 The type of isostatic compensation depends on the flexural rigidity of the supporting material. a) *Local isostasy*. Where there is no rigidity, compensation is directly below the load. b) *Regional isostasy*. Materials with rigidity are flexed, distributing the load over a broader region.

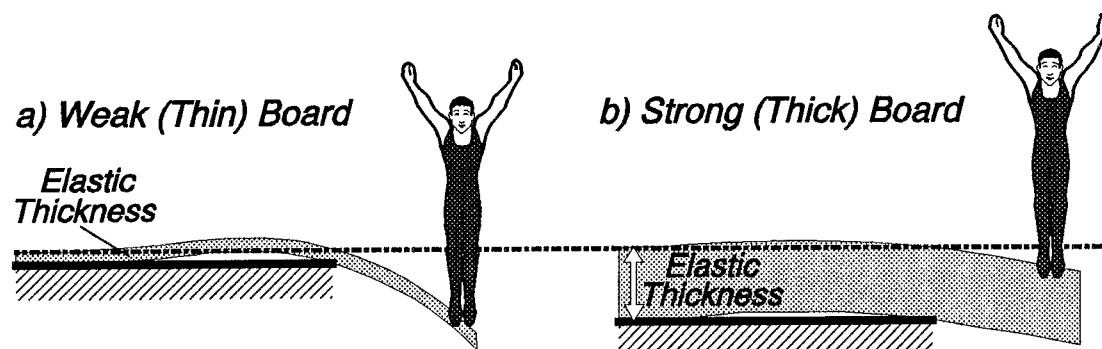


FIGURE 8.22 Flexural rigidity. a) A thin diving board (small elastic thickness) has low flexural rigidity. b) A thick board (large elastic thickness) has high flexural rigidity.

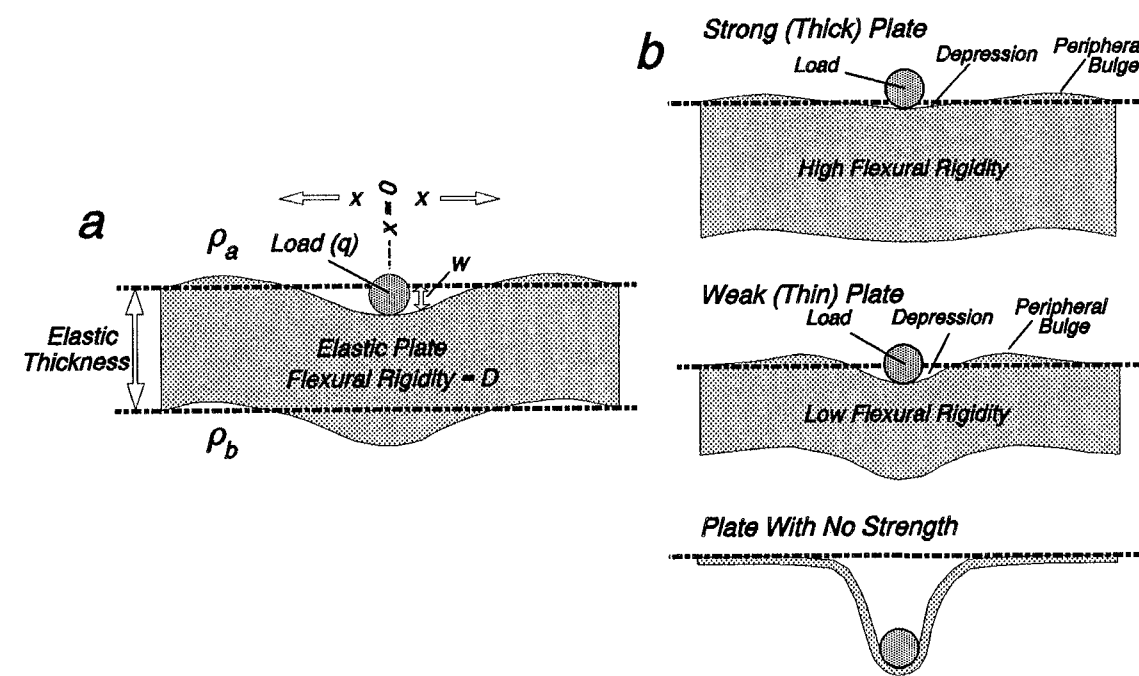


FIGURE 8.23 a) Parameters for two-dimensional model of a plate flexed by a linear load. Both the plate and load extend infinitely in and out of the page. See text for definition of variables. b) Positions of depressions and bulges formed on the surface of a flexed plate. A strong plate has shallow but wide depressions. The depressions and peripheral bulges have larger amplitudes on a weak plate, but are closer to the load. A very weak plate collapses into local isostatic equilibrium.

The deflection of a two-dimensional plate, due to a linear load depressing the plate's surface, is developed by Turcotte and Schubert (1982). The model (Fig. 8.23a) assumes that material below the plate is fluid. The vertical deflection of points along the surface of the plate can be computed according to:

$$D(\frac{d^4w}{dx^4}) + (\rho_b - \rho_a)gw = q(x)$$

where:

D = flexural rigidity of the plate

w = vertical deflection of the plate at x

x = horizontal distance from the load to a point on the surface of the plate
 ρ_a = density of the material above the plate
 ρ_b = density of the material below the plate
 g = gravitational acceleration
 $q(x)$ = load applied to the top of the plate at x .

Four important concepts are illustrated by solutions to the above equation (Fig. 8.23b): 1) a strong lithospheric plate (large D) will have a small amplitude deflection (small w), spread over a long wavelength; 2) a weak lithospheric plate (small D) has large deflection (large w), but over a smaller wavelength; 3) where plates have significant strength, an upward deflection ("peripheral" or "flexural" bulge) develops some distance from the load, separated by a depression; 4) plates with no strength collapse into local isostatic equilibrium.

Two simplified examples of lithospheric flexure are shown in Fig. 8.24. At a subduction zone (Fig. 8.24a), flexure is analogous to the bending at the edge of a diving board (Fig. 8.22). The load is primarily the topography of the accretionary wedge and volcanic arc on the overriding plate. Flexure of the downgoing plate results in a depression (trench) and, farther out to sea, a bulge on the oceanic crust. The mass of high mountains puts a load on a plate that can be expressed in both directions (Fig. 8.24b). Depressions between the mountains and flexural bulges ("foreland basins") can fill with sediment to considerable thickness.

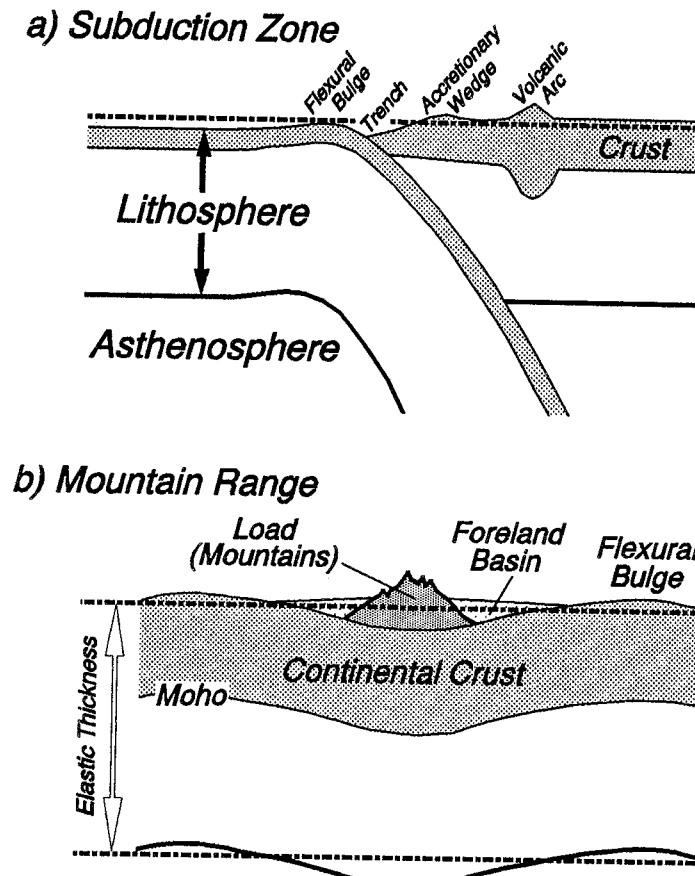


FIGURE 8.24 Examples of lithospheric flexure. a) A flexural bulge and depression (trench) develop as the downgoing plate is flexed at a subduction zone. b) The weight of a mountain range causes adjacent depressions that fill with sediment (foreland basins).

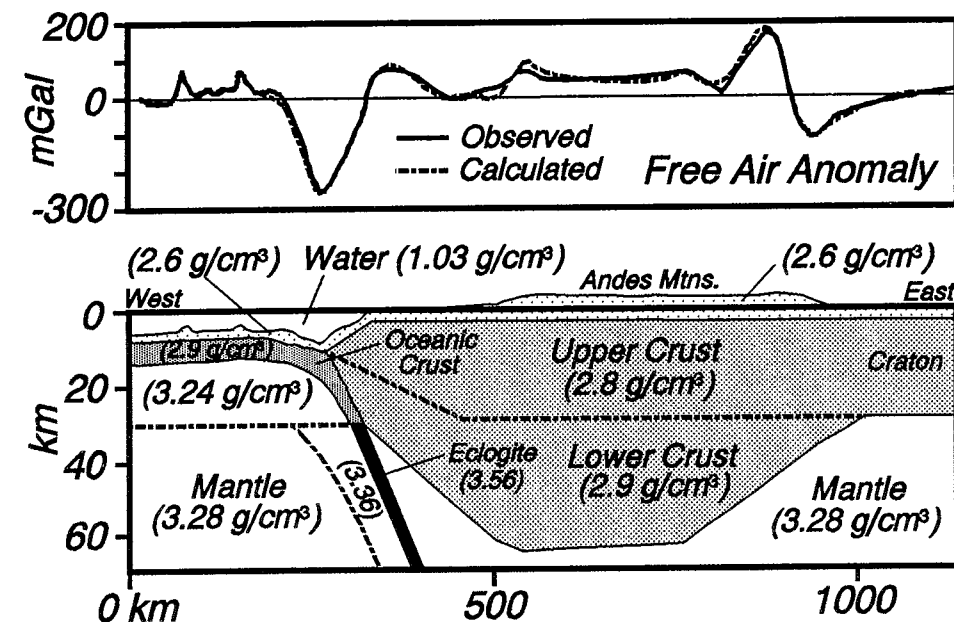


FIGURE 8.39 Observed and modeled free air gravity anomaly of the Andes Mountains and adjacent regions, showing the east portion of the classic “Batman anomaly.” The model shown results in a calculated anomaly in close agreement with the observed. Densities in g/cm^3 ($= 10^3 \text{ kg}/\text{m}^3$). From J. Grow and C. Bowin, *Journal of Geophysical Research*, vol. 80, pp. 1449–1458, © 1975. Redrawn with permission of the American Geophysical Union, Washington, D.C.

TECTONIC SETTINGS AND THEIR GRAVITY EXPRESSIONS

The gross forms of free air and Bouguer gravity anomalies reflect: 1) the *density distribution* of Earth materials in a region; and 2) the *flexural strength* of the materials. The Airy isostatic model is an end-member case where supporting materials have no flexural strength. While an oversimplification, the Airy model is nonetheless useful in understanding the general form of gravity anomalies. Once those simple forms are appreciated, modeling of other parameters can be attempted (flexural strength, complex density distributions).

The Airy model suggests isostatic balance involving two boundaries: 1) the *topography* and/or *bathymetry*; and 2) the *crust/mantle boundary (Moho)*. Those boundaries are important because they are universal and represent large density contrasts. In some regions, a third boundary is a significant element in isostatic balance: 3) the *lithosphere/asthenosphere boundary*.

The Airy isostatic model in Fig. 8.20 can be modified to incorporate all three boundaries, as summarized below and illustrated in Fig. 8.40. At the *depth of compensation* beneath each region, two equations hold true. 1) The total *pressure* (P) exerted by any vertical column (divided by g) is equal to that of any other vertical column:

$$\rho/g = \rho_a h_a + \rho_w h_w + \rho_c h_c + \rho_m h_m + \rho_A h_A = \text{Constant}$$

where:

$$\rho_a = \text{density of the air } (\rho_a \approx 0)$$

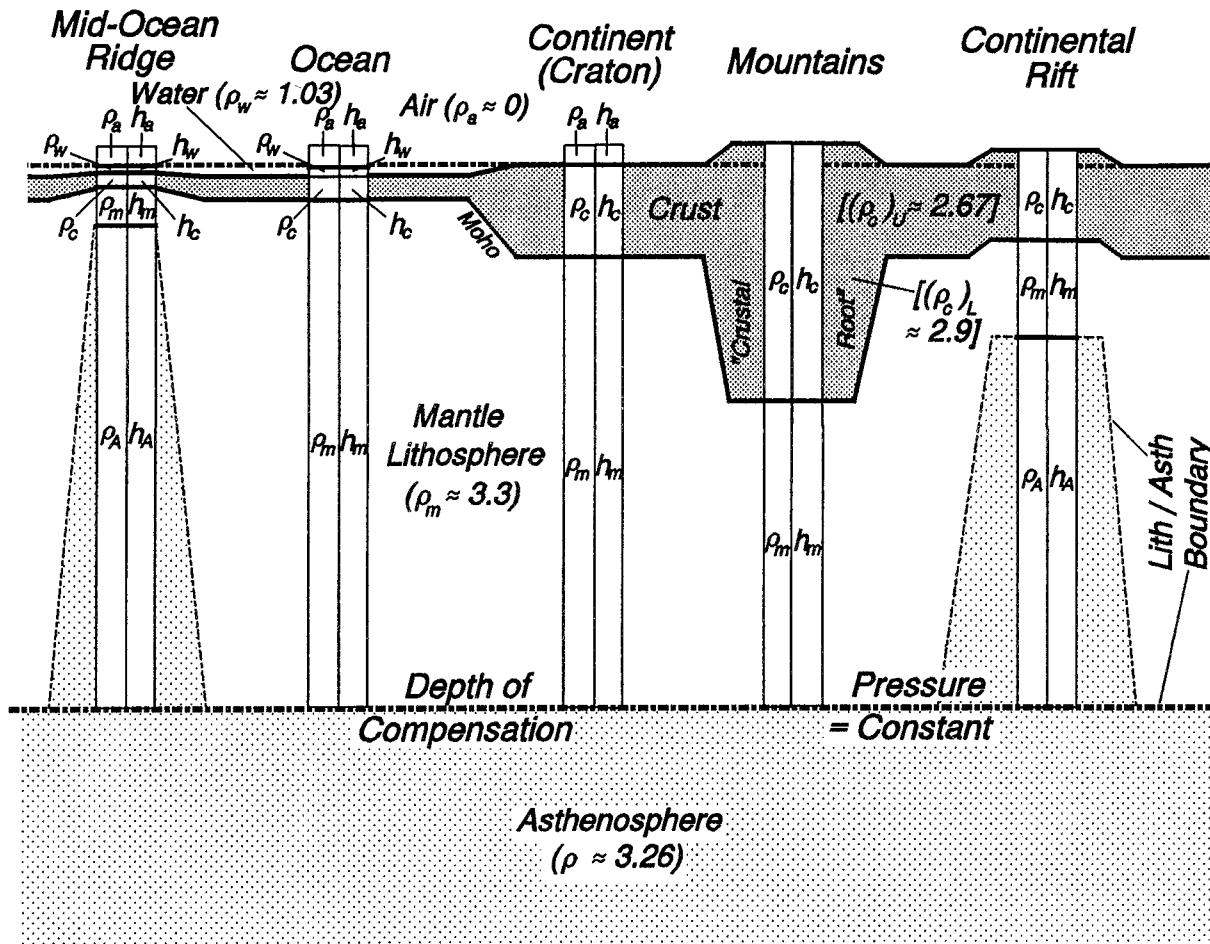


FIGURE 8.40 Airy isostatic model, modified to include lithosphere/asthenosphere boundary. See text and subsequent figure captions for definition of parameters. Note that h_c in continental areas is the depth to the Moho below the sea level datum, plus the height of the topography (h_t in subsequent figures). There is a slight drop in density across the lithosphere/asthenosphere boundary; elevated asthenosphere thus provides buoyancy, supporting the weight of uplifted topography and mantle at continental rifts and mid-ocean ridges.

h_a = thickness of the air column

ρ_w = density of the water

h_w = thickness of the water column

ρ_c = density of the crust

h_c = thickness of the crust

ρ_m = density of the mantle part of the lithosphere

h_m = thickness of the mantle part of the lithosphere

ρ_A = density of the asthenosphere

h_A = thickness of the asthenosphere column.

2) The total *thickness* (T) of any vertical column is equal to that of any other vertical column:

$$T = h_a + h_w + h_c + h_m + h_A = \text{Constant}$$

Gravity Anomalies for Regions in Local Isostatic Equilibrium

The models below comprise five tectonic settings. Each setting has characteristic heights of topography (bathymetry) and thicknesses of the crust and entire lithosphere.

1. *Continental Craton*: Topography near sea level; crust and lithosphere of normal thickness.
2. *Continental Rift*: Uplifted topography; thin crust and thin lithosphere.
3. *Continental Margin*: Drop in topography; transition from thicker continental to thinner oceanic crust.
4. *Mid-Ocean Ridge*: Shallower water than normal ocean; thin oceanic crust and thin lithosphere.
5. *Mountain Range*: High topography; thick crust.

The settings are related, in that: a) as a *craton* rips apart the crust and the entire lithosphere thin, forming a *continental rift* zone (Fig. 2.13); b) rifting can continue to the point where new oceanic lithosphere is created, forming an ocean basin with a *mid-ocean ridge* in the center and passive *continental margins* on the sides (Fig. 2.14); c) the basin can close through subduction of the oceanic lithosphere, resulting in collision of the continental margins and thickening of the crust as a *mountain range* forms (Fig. 2.18).

The continental margin and mountain range on the model (Fig. 8.40) are similar to those in previous models (Figs. 8.32, 8.36). Their respective gravity expressions are also similar, because when those features are old, there may be no significant relief on the lithosphere/asthenosphere boundary. The same can be said for a continental craton. Gravity modeling assuming normal Airy isostasy, where compensation is achieved at the depth of the deepest Moho (Fig. 8.20), is often sufficient to illustrate the forms of free-air and Bouguer anomalies in those three settings.

In areas of active plate divergence (continental rifts; mid-ocean ridges), gravity anomalies cannot be explained adequately without considering relief on the lithosphere/asthenosphere boundary. Note that the asthenosphere is less dense than the overlying, mantle part of the lithosphere, so that: 1) the asthenosphere column represents mass deficit ($-\Delta m$), relative to the mantle part of the lithosphere ($+\Delta m$); 2) the density contrast between the asthenosphere and the mantle part of the lithosphere is small, so that large relief on the lithosphere/asthenosphere boundary is required to compensate mass excesses due to topography and crustal thinning.

In active convergent plate settings, the lithosphere/asthenosphere boundary also needs to be considered in modeling gravity anomalies. In the Alps, for example, a lithosphere root is an important component of isostatic balance, contributing 30 to 50 *mGal* to the observed gravity anomalies (Kissling et al., 1983; Lillie et al., 1994). At subduction zones, the mantle of the downgoing plate comprises a mass excess that needs to be accounted for in gravity models as well as models of isostatic equilibrium and lithosphere flexure (Grow and Bowin, 1975).

The models below show contributions to gravity anomalies due to compensatory changes in topography (bathymetry), Moho depth, and lithosphere/asthenosphere boundary depth, for simplified models of the five tectonic settings. Density assumptions are:

$$\text{Air: } \rho_a = 0$$

$$\text{Water: } \rho_w = 1.03 \text{ g/cm}^3$$

$$\text{Upper crust: } (\rho_c)_U = 2.67 \text{ g/cm}^3$$

$$\text{Lower crust: } (\rho_c)_L = 2.9 \text{ g/cm}^3$$

$$\text{Mantle part of Lithosphere: } \rho_m = 3.3 \text{ g/cm}^3$$

$$\text{Asthenosphere: } \rho_A = 3.26 \text{ g/cm}^3$$

In gravity modeling, important effects are due to *lateral* changes in mass (Δm), reflected by *density contrasts* across boundaries ($\Delta\rho$). Zones of significant density contrast, bounded by the three fundamental boundaries, are therefore:

1. Shallow effects:

a) Mass above sea level vs. air (topography):

$$\Delta\rho = (\rho_c)_U - \rho_a = +2.67 \text{ g/cm}^3.$$

b) Ocean water vs. upper crust (bathymetry):

$$\Delta\rho = \rho_w - (\rho_c)_U = -1.64 \text{ g/cm}^3.$$

2. Mantle vs. lower crust (Moho):

$$\Delta\rho = \rho_m - (\rho_c)_L = +0.4 \text{ g/cm}^3.$$

3. Asthenosphere vs. mantle part of lithosphere (lithosphere/asthenosphere boundary):

$$\Delta\rho = \rho_A - \rho_m = -0.04 \text{ g/cm}^3.$$

For each of the five models, contributions to gravity due to the change in depth to each of the boundaries are calculated. The *free air anomaly* is then computed as the sum of the three contributions. Density contrasts chosen for the topographic and bathymetric effects are exactly the same as those commonly used for Bouguer corrections (Fig. 8.12); the *Bouguer anomaly* is therefore the sum of the contributions without the topographic and bathymetric effects.

The models start with a continental craton, constructed with these simplifying assumptions: 1) the surface of the craton is at sea level; 2) the Moho is at a depth of 33 km; 3) the lithosphere/asthenosphere boundary is at 180 km depth. The series of models can be viewed as a progression of ripping the craton apart (continental rift zone), opening an ocean basin (continental margins and mid-ocean ridge), then closing the ocean and colliding the continental fragments (mountain range). This progression is the “Wilson Cycle,” portrayed in Figs. 2.14 to 2.18.

The three fundamental boundaries change depth in each model so that, at the depth of compensation (180 km), the pressure is the same as it was for the starting craton. Contributions to gravity result from changes in depth of the three boundaries, relative to each contribution equal to zero for the craton. A composite model then shows a comparison of the amplitudes and forms of free air and Bouguer gravity anomalies in the different tectonic settings.

1. Continental Craton Fig. 8.41 is a simplified version of the lithosphere of a stable continental craton. The model incorporates a 180 km thick lithosphere; 180 km is thus chosen as the standard depth of compensation for the other models. The model surface is at sea level, so there is no topographic contribution to gravity. Likewise, the Moho and lithosphere/asthenosphere boundaries are flat, resulting in no form to their gravity contributions. Changes in depths to these three boundaries result in positive or negative contributions to gravity anomalies in the other models.

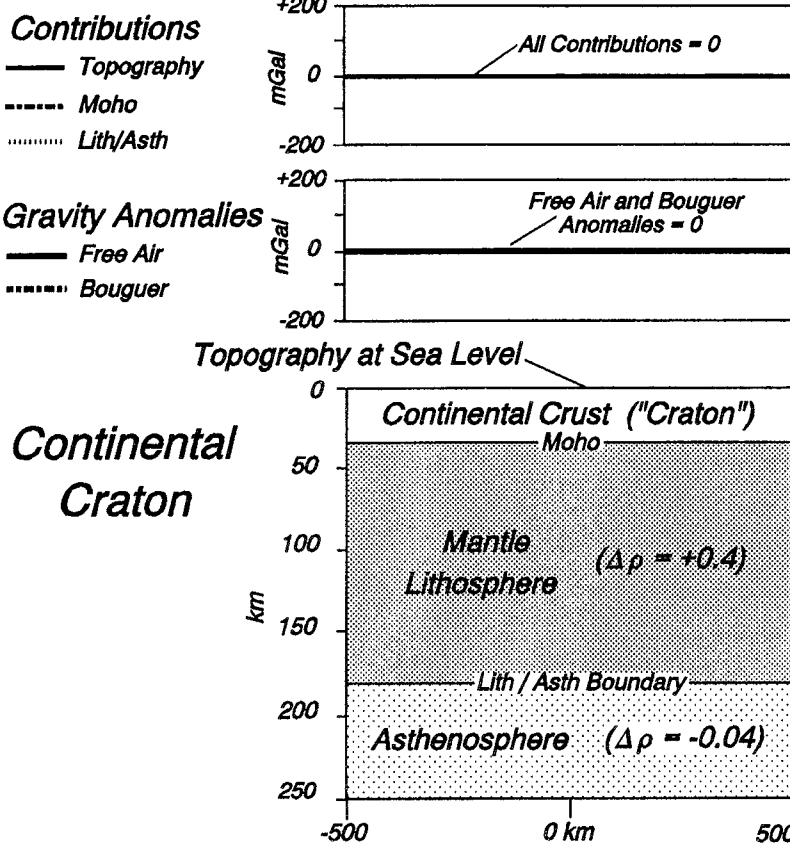


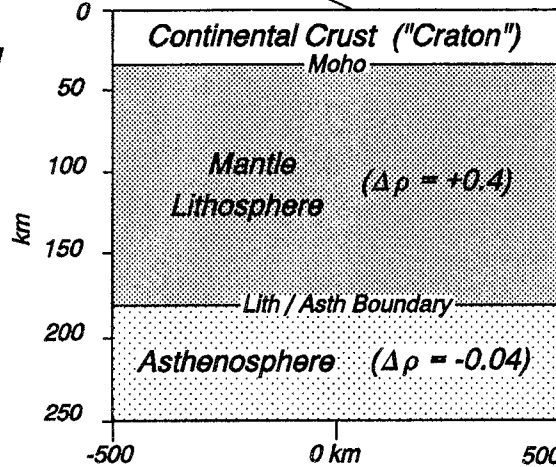
FIGURE 8.41 Gravity expression of normal continental lithosphere. Parameters for the model are (see Fig. 8.40):

h_t = height of topography = 0
 h_c = thickness of crust = 33 km
 h_m = thickness of mantle part of lithosphere = 147 km.

The model arbitrarily assumes that this configuration results in zero amplitude free air and Bouguer gravity anomalies. (In reality, the topography of a craton is tens to a few hundred meters above sea level, resulting in slightly negative Bouguer anomalies). The 180 km depth of compensation is maintained throughout the series of models in the next few figures.

Topography at Sea Level

Continental Craton



2. Continental Rift At a continental rift (Fig. 8.42), both the crust and entire lithospheric plate thin. Elevated asthenosphere can be viewed as an “inflated balloon,” its buoyancy supporting the weight of elevated mantle and, in some cases, topography. Note that the negative density contrast across the lithosphere/asthenosphere boundary ($\Delta\rho = -0.04 \text{ g/cm}^3$) is far less than the positive contrasts for the topography ($\Delta\rho = +2.67 \text{ g/cm}^3$) and the Moho ($\Delta\rho = +0.4 \text{ g/cm}^3$). The relief on the lithosphere/asthenosphere boundary (130 km) is thus far greater than the combined relief of the other boundaries (4.5 km).

The topography and the elevated mantle beneath the thin crust result in positive gravity contributions of relatively steep gradient. The compensatory mass deficit of the elevated asthenosphere is a deep effect, giving a much broader gravity low that does not reach full amplitude. The free air gravity anomaly (sum of the three effects) is a high over the rift, with flanking lows. When the effect of mass above sea level (topographic contribution) is removed, the Bouguer anomaly is a broad low reflecting the elevated asthenosphere.

The Basin and Range Province in the western United States illustrates the pattern of free air and Bouguer gravity anomalies shown in Fig. 8.42. The asthenosphere is so shallow that there is very little mantle lithosphere, as indicated by low seismic velocities (Fig. 4.15, 4.19a) and low Bouguer anomalies (Fig. 8.43a). Hot asthenosphere at shallow depth is under such low pressure that partial melting occurs (Figs. 2.7, 2.24b). The resulting gabbroic magma can underplate the continental crust, establishing a new, flat Moho. This interpretation is consistent with obser-

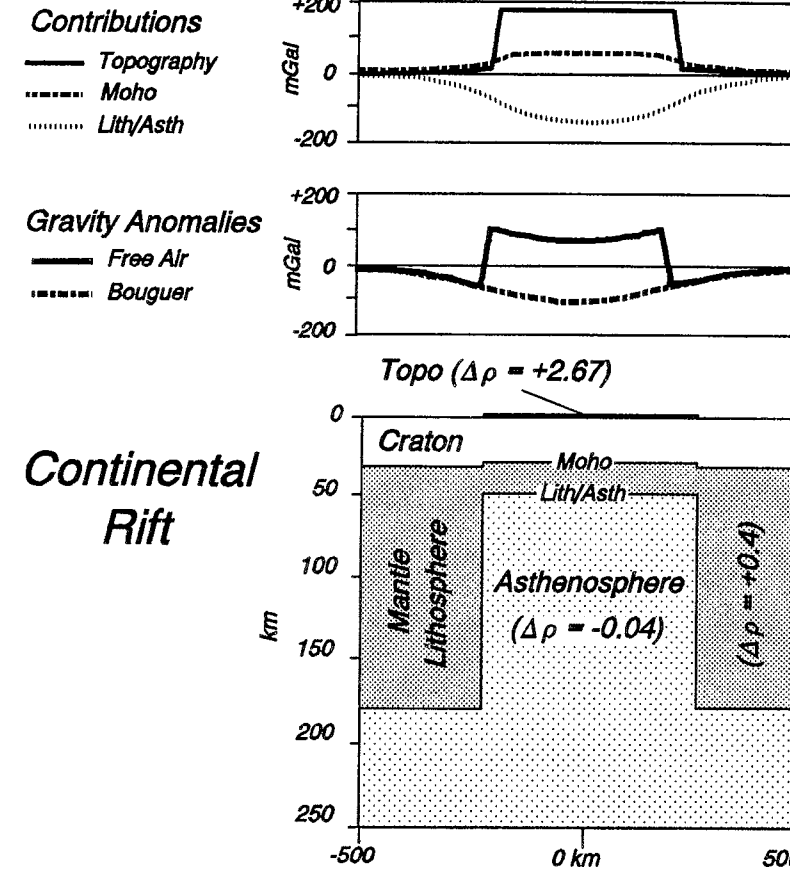


FIGURE 8.42 Local isostatic model, showing free air and Bouguer gravity anomalies at a continental rift zone.

Density contrasts, in g/cm^3 , are: +2.67 for the mass above sea level relative to air; +0.4 for the mantle lithosphere relative to the lower crust; and -0.04 for the asthenosphere relative to the mantle lithosphere. The depth of compensation (180 km) is the same as in the starting craton model (Fig. 8.41). Parameters for the model are:

At the rift:

h_t = height of topography = 1.5 km
 h_c = thickness of crust = 31.5 km (Moho depth = 30 km)
 h_m = thickness of mantle part of lithosphere = 19.875 km
 h_A = thickness of asthenosphere column = 130.125 km.

Outside the rift (normal continental lithosphere):

$h_t = 0$
 $h_c = 33 \text{ km}$
 $h_m = 147 \text{ km}$
 $h_A = 0$.

vations of prominent reflections from a horizontal Moho at about 30 km depth beneath much of the Basin and Range Province (Figs. 6.23, 6.24).

Continental rifts have a wide variety of crustal and lithospheric structure and, hence, a variety of free air and Bouguer gravity anomalies. The Pannonian Basin in central Europe is broad, like the Basin and Range Province, but it has thinner crust ($\approx 25\text{--}30 \text{ km}$) and less relief on the lithosphere/asthenosphere boundary (Babuška et al., 1988; Šefara, 1986). The region is thus a topographic depression. Free air anomalies have a form similar to that shown in Fig. 8.42, but with much smaller amplitude; the Bouguer anomaly is a broad, low-amplitude high reflecting the Moho relief (Bielik, 1988; Lillie et al., 1994).

The East African rift zone is narrower than the Basin and Range Province or Pannonian Basin rifts. The Bouguer gravity anomaly low is prominent, resulting from very shallow asthenosphere (Fig. 8.43b). Superimposed on the low is a high of about 50 mGal, interpreted to be caused by high density (gabbroic?) material intruded throughout the rift valley crust.

At very old continental rift zones, cooling transforms the density of the elevated asthenosphere back to that of normal mantle lithosphere; the lithosphere/asthenosphere boundary thus flattens back to normal continental depths. Intruded gabbro cools and densifies, weighting down the crust, causing it to sag. An example is the 1.1 billion-year-old Keweenawan Rift in the central United States (Fig. 8.43c). The Bouguer gravity anomaly is a broad low reflecting the sagging crust and

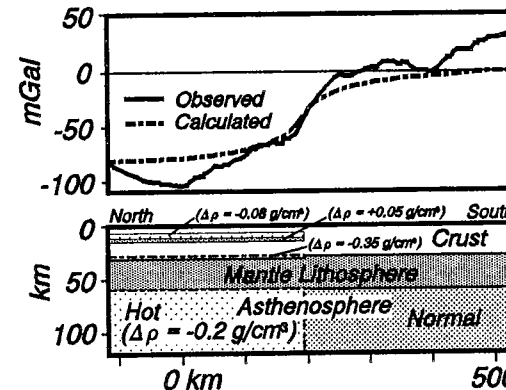
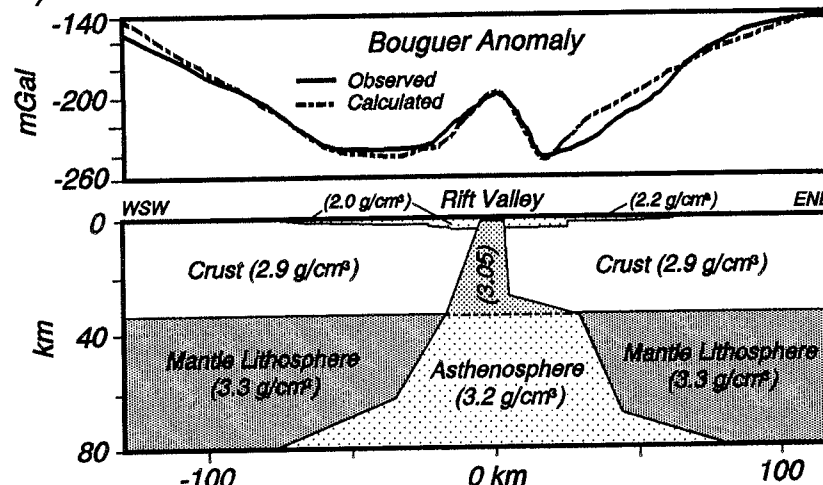
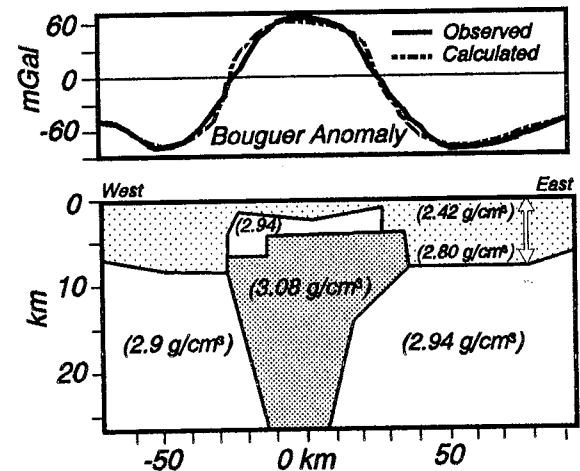
a) Basin and Range Province**b) East African Rift****c) Keweenawan Rift**

FIGURE 8.43 Bouguer gravity anomalies at continental rifts, along with interpreted density models. a) *Basin and Range Province* from southern California to central Nevada. From R. Saltus and G. Thompson, *Tectonics*, vol. 14, pp. 1235–1244, © 1995. Redrawn with permission of the American Geophysical Union, Washington, D.C. Observed curve is a residual anomaly, whereby effects of Cenozoic basins were removed from the complete Bouguer anomaly. Low values around -100 mGal reflect shallow, hot asthenosphere that supports the weight of the higher topography on the north side of the section. b) *East African Rift*. From “The geology of the Eastern Rift System of Africa,” by B. Baker, P. Mohr, and J. Williams, GSA Special Paper, No. 136, 67 pp., © 1972. Redrawn with permission of the Geological Society of America, Boulder, Colorado, USA. A Bouguer gravity maximum, due to high density material intruding the crust, is superimposed on the asthenosphere minimum. c) *Keweenawan Rift* in Iowa and Nebraska, central United States. From L. Ocola and R. Meyer, *Journal of Geophysical Research*, vol. 78, pp. 5173–5194, © 1973. Redrawn with permission of the American Geophysical Union, Washington, D.C. The prominent high results from relatively high-density (3.08 g/cm^3) material extending through the crust, perhaps gabbro solidified within this 1.1 billion-year-old rift (compare with modern rift in b).

sedimentary infill of rift basins; a superimposed gravity high results from gabbro that intruded the crust along the rift axis (Serpa et al., 1984).

3. Passive Continental Margin In a fully evolved ocean basin, passive continental margins are far from a mid-ocean ridge (Fig. 2.14c). The region cools through time, so that there may be no significant relief left on the thermally controlled, lithosphere/asthenosphere boundary (Fig. 8.44). Substantial change in depth remains on the Moho, which is a chemical boundary (Figs. 2.3, 4.9). The free air and Bouguer gravity anomalies at a fully evolved passive margin are therefore of the form and amplitude shown in Figs. 8.33 to 8.35; isostatic compensation and gravity anomalies result from balance between mass excess of the extra mantle beneath the thin oceanic crust and the overlying, low-density water column.

4. Mid-Ocean Ridge The isostatic situation for a mid-ocean ridge (Fig. 8.45) is similar to that depicted for a continental rift zone (Fig. 8.42). The density deficiency

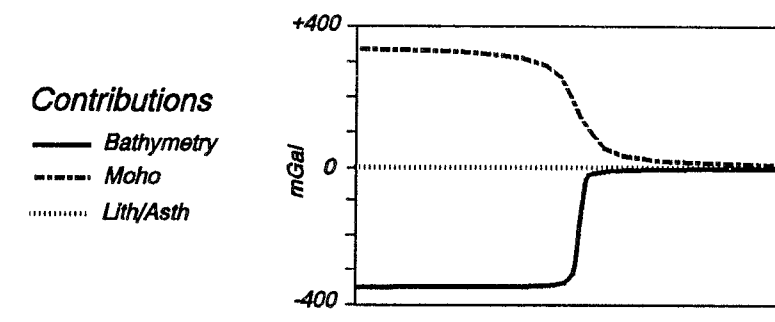


FIGURE 8.44 Contributions of three fundamental boundaries and resulting gravity anomalies for a passive continental margin in local isostatic equilibrium. Parameters used in the model are:

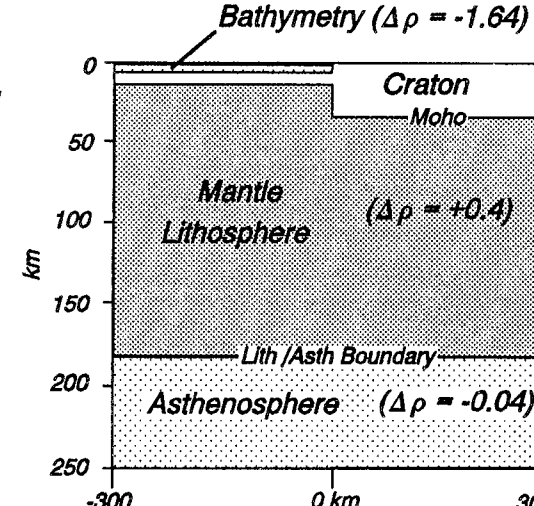
Normal oceanic lithosphere:
 $h_w = \text{thickness of water column} = 5 \text{ km}$
 $h_c = \text{thickness of crust} = 7.5 \text{ km}$
(Moho depth = 12.5 km)
 $h_m = \text{thickness of mantle part of lithosphere} = 167.5 \text{ km}.$

Normal continental lithosphere:
 $h_w = 0$
 $h_c = 33 \text{ km}$
 $h_m = 147 \text{ km}.$

Density contrasts are nearly identical to those used in the earlier passive margin model (Figs. 8.32 to 8.34), and there is no relief on the lithosphere/asthenosphere boundary; free air and Bouguer gravity anomalies are essentially the same as in the earlier model.

Gravity Anomalies

- Free Air
- Bouguer



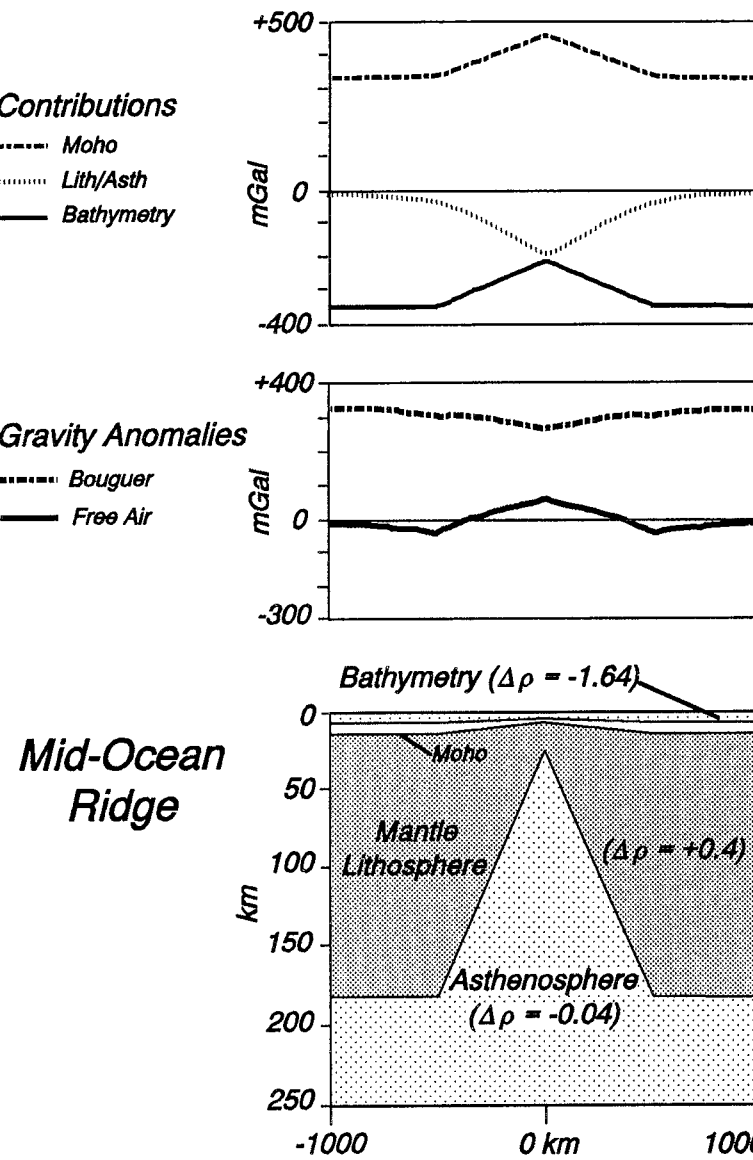


FIGURE 8.45 Contributions of three fundamental boundaries and resulting gravity anomalies for a mid-ocean ridge in local isostatic equilibrium. The depth of compensation is 180 km. Model parameters are:

On the ridge:

h_w = thickness of water column = 3 km
 h_c = thickness of crust = 2 km (Moho depth = 5 km)
 h_m = thickness of mantle part of lithosphere = 18.0 km
 h_A = thickness of asthenosphere column = 157.0 km.

Away from the ridge (normal oceanic lithosphere):

h_w = 5 km
 h_c = 7.5 km (Moho depth = 12.5 km)
 h_m = 167.5 km
 h_A = 0.

The Moho contribution is more than +300 mGal, because the region has thin crust, relative to the standard, continental craton (Figs. 8.40, 8.41; compare to the seaward portion of the passive margin model, Fig. 8.44). Likewise, the bathymetric contribution has background values less than -300 mGal.

of the elevated asthenosphere supports the weight of the ridge and elevated mantle. The positive changes in gravity across the ridge from the Moho and bathymetry are superimposed on a broad low resulting from the deep effect of the asthenosphere. The resulting free air gravity anomaly thus displays a high with flanking lows.

After effectively removing the bathymetric contribution, the Bouguer anomaly shows the more than 300 mGal background level associated with oceanic crust (see Bouguer anomaly for the passive continental margin in Figs. 8.34 and 8.44). There is a drop in Bouguer anomaly values over the ridge, due to the elevated asthenosphere.

Fig. 8.46 shows free air and Bouguer gravity anomalies observed across the Mid-Atlantic Ridge. Short-wavelength highs and lows mimic the topographic relief on the sea floor, which is uncompensated. The longer wavelength anomalies show widths and amplitudes that are in general agreement with those computed in

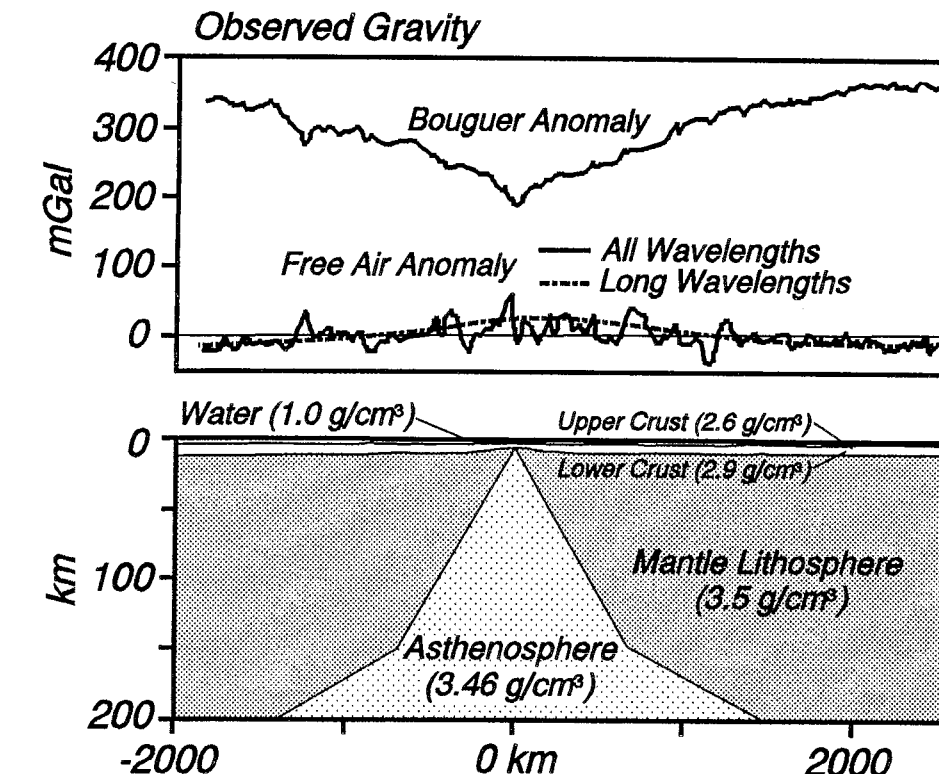


FIGURE 8.46 Free air and Bouguer gravity anomalies observed across the Mid-Atlantic Ridge (Talwani et al., 1965). Densities in model are in g/cm^3 ($= 10^3 \text{ kg}/\text{m}^3$). Interpreted density distribution (Keen and Tramontini, 1970) shows shallow asthenosphere with density contrast of $-0.04 \text{ g}/\text{cm}^3$, relative to adjacent mantle lithosphere. Compare observed gravity anomalies and lithosphere structure with Fig. 8.45. From M. Talwani, X. Le Pichon, and M. Ewing, *Journal of Geophysical Research*, vol. 70, pp. 341–352, © 1965. Redrawn with permission of the American Geophysical Union, Washington, D.C.

Fig. 8.45; the free air anomaly shows a broad central high with flanking lows, and the Bouguer anomaly reveals a decrease associated with the shallow asthenosphere. The modeled lithosphere structure for the Mid-Atlantic Ridge thus suggests local isostatic equilibrium, the hot asthenosphere supporting the weight of the topography and elevated mantle at the ridge.

5. Mountain Range The lithosphere/asthenosphere boundary generally has little relief left as a mountain range ages, so that the topography and supporting crustal root are the major contributions to gravity anomalies (Fig. 8.47). The density contrast of the topography compared to air ($\approx +2.67 \text{ g}/\text{cm}^3$) is generally 5 to 8 times that of the crustal root compared to surrounding mantle ($\approx -0.4 \text{ g}/\text{cm}^3$); crustal roots must therefore be 5 to 8 times as thick as the topographic relief of a mountain range. In the Himalaya Mountains and adjacent Tibetan Plateau, for example, the 4.5 km elevation of the region is supported by crust that is about 30 km thicker than normal.

For some mountain ranges it is essential to consider relief on the lithosphere/asthenosphere boundary (for example, the Alps in Europe and Sierra Nevada in the United States). Those ranges are so young that there is still a root of lithosphere left from the plate convergence that formed the mountains (Fig. 2.16b).

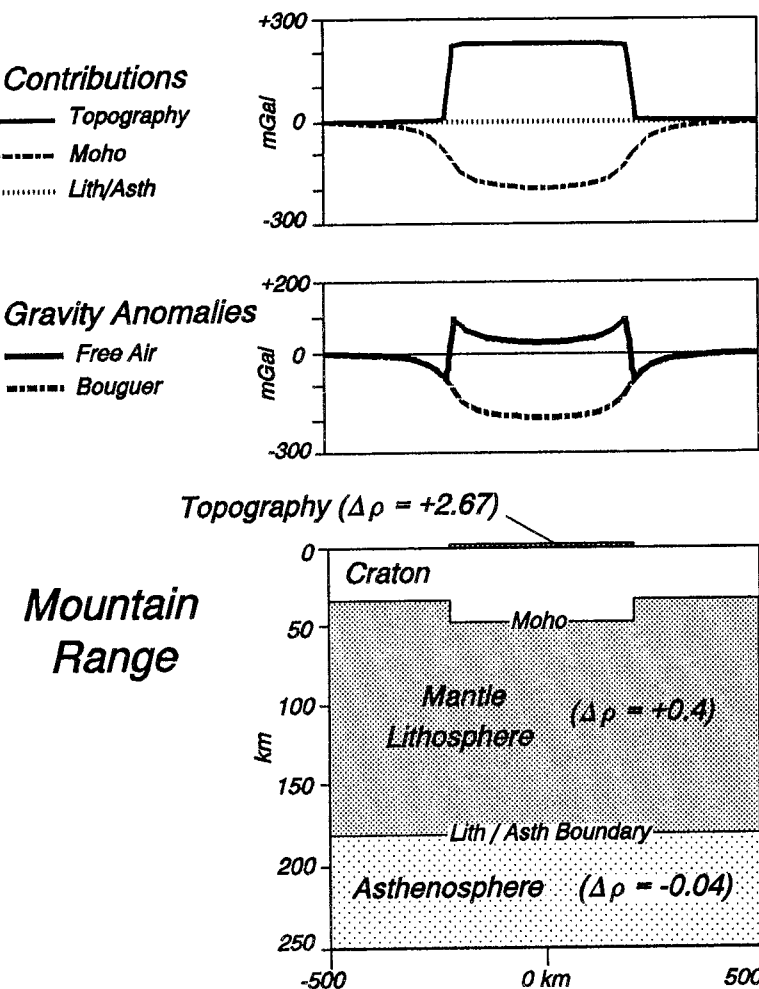


FIGURE 8.47 General form of free air and Bouguer gravity anomalies at a mountain range. Parameters are:

At the mountains:

h_t = height of topography = 2 km
 h_c = thickness of crust = 48.35 km
(Moho = 46.35 km deep)
 h_m = thickness of mantle part of lithosphere = 133.65 km.

Outside the mountains (normal continental lithosphere):

h_t = 0
 h_c = 33 km
 h_m = 147 km.

In an old mountain range the thermally controlled, lithosphere/asthenosphere boundary equilibrates to a horizontal surface. Free air and Bouguer anomalies thus reveal the classic "Batman anomaly," because the major contributions are from the topography and its supporting crustal root (Fig. 8.38).

for the Sierra Nevada; Fig. 2.18 for the Alps). In such cases, the lithosphere roots represent mass excesses that lessen the topographic relief.

Composite Model The composite model (Fig. 8.48) shows general forms of contributions, and free air and Bouguer gravity anomalies, at each of the five tectonic settings. The figure is important because it represents the "background" (or "regional") anomalies that one should appreciate before modeling and interpreting gravity anomalies in a particular setting. By understanding the major contributions for a local isostatic situation, one can then analyze problems of mass distribution and lithospheric strength in terms of deviation from local isostasy.

Gravity Anomaly Maps

Gravity anomaly maps present information useful to understanding density distribution and isostatic state of a region. An ideal situation would be to analyze, together, maps of: 1) *topography* (see front inside cover of this book); 2) *surface geology*; 3) *sediment thickness and intra-crustal structure* based on drilling and seismic reflection profiles (Figs. 6.23 to 6.39); 4) *Moho depths* from refraction surveys

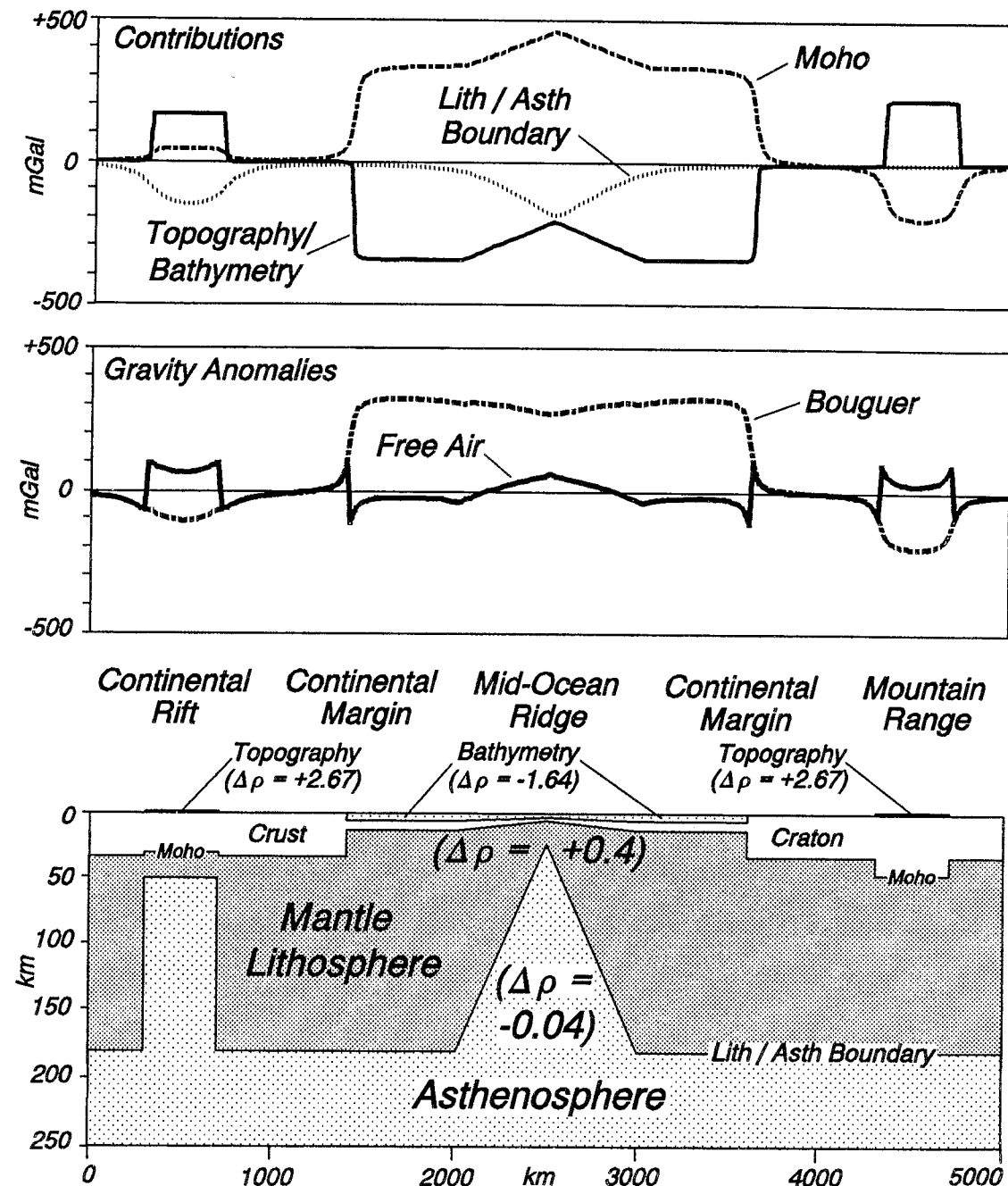


FIGURE 8.48 Composite model of local isostatic equilibrium, showing all five tectonic settings from the previous series of illustrations. The depth of compensation is the depth of the deepest lithosphere (180 km). Density contrasts ($\Delta\rho$ in g/cm³) are for topography relative to air; bathymetry relative to upper crust; mantle lithosphere relative to lower crust; asthenosphere relative to mantle lithosphere. Note that the contributions from the three critical boundaries lead to free air anomalies near zero, except at edge effects. The fact that the positive and negative areas under the curve sum to zero illustrates local isostasy. The Bouguer gravity anomaly generally follows the form of the Moho, staying near zero over the cratons, rising over the thin oceanic crust, and falling where the crust is thick beneath the mountain range. Bouguer lows also reflect asthenosphere elevated beneath continental rifts and mid-ocean ridges. The inverse relationship between Bouguer anomaly and topography/bathymetry is apparent: high values occur where bathymetry is deep in the ocean; relative lows are associated with surface relief at the continental rift, mid-ocean ridge, and mountain range.

(Figs. 4.16 to 4.19); 5) depths to the lithosphere/asthenosphere boundary from seismic delay time/tomography methods (Fig. 7.34); 6) free air gravity anomaly; 7) Bouguer gravity anomaly. Constraints on densities come from surface sample and borehole measurements, as well as approximations based on seismic velocities (Fig. 3.10). Incorporation of all of these data would more likely result in cross-sectional interpretations that honor geological reality (first order constraints, Fig. 1.8), and that consider the state of isostasy.

North America The gravity anomaly map of North America (back inside cover of this book) presents free air anomalies at sea and Bouguer anomalies on land. The anomalies correspond at the shoreline, because the Bouguer correction at sea level is zero. Several prominent features are evident; most can be interpreted in terms of the isostatic model in Fig. 8.48.

1. Near-zero values occur over the continental craton, comprising most of the eastern parts of Canada and the United States (Fig. 8.41).
2. Low Bouguer values are coincident with the high topography and crustal root of the Rocky Mountains, extending from western Mexico to western Canada (Figs. 4.16, 8.38, 8.47).
3. A broad Bouguer low occurs over the Basin and Range Province, caused by shallow asthenosphere (Figs. 8.42, 8.43a).
4. A prominent gravity high runs through the central United States, caused by gabbro intruded into the crust along the failed, 1.1 billion-year-old Keweenawan rift (Fig. 8.43c).
5. Free air edge effects are prominent near the shelf edge off the east coast of Canada and the United States, representing the transition from thick continental to thinner oceanic crust of the passive margin (Figs. 8.34, 8.35).
6. Edge effects also occur along transitions from thicker (continental or island arc) to thinner (oceanic) crust at subduction zones, although modified by deviations from local isostasy (see left side, Fig. 8.39). At the Alaska Peninsula and Aleutian island arc, effects of a rigid lithosphere accentuate the highs and lows of the free air anomaly, and a flexural bulge high occurs seaward of the trench. Similar effects are observed in the Lesser Antilles arc in the Caribbean region, and along the Pacific coast of Mexico.
7. The Mid-Atlantic Ridge segment south of Iceland displays a broad low split by a central high, characteristic of free air anomalies across a mid-ocean ridge (Figs. 8.45, 8.46).

Central Europe Prominent features evident from the Bouguer gravity anomaly map of central Europe (Fig. 8.49) include: 1) a narrow, low-amplitude minimum associated with a downwarped “keel” on the Moho, formed during an early stage of continental collision in the Carpathians (Fig. 8.50b); 2) a broad low representing a crustal root beneath the eastern Alps, a consequence of a more advanced stage of continental collision (Fig. 8.50c); 3) a circular high representing shallow mantle beneath the Pannonian Basin (Fig. 8.51).

Deviations from Local Isostasy

Lithospheric plate strength partially supports the weight of topographic and subsurface loads. Gravity anomalies resulting from the two examples presented earlier in this chapter (Fig. 8.24) can be studied in the context of how they deviate from anomalies caused by simple Airy isostasy.

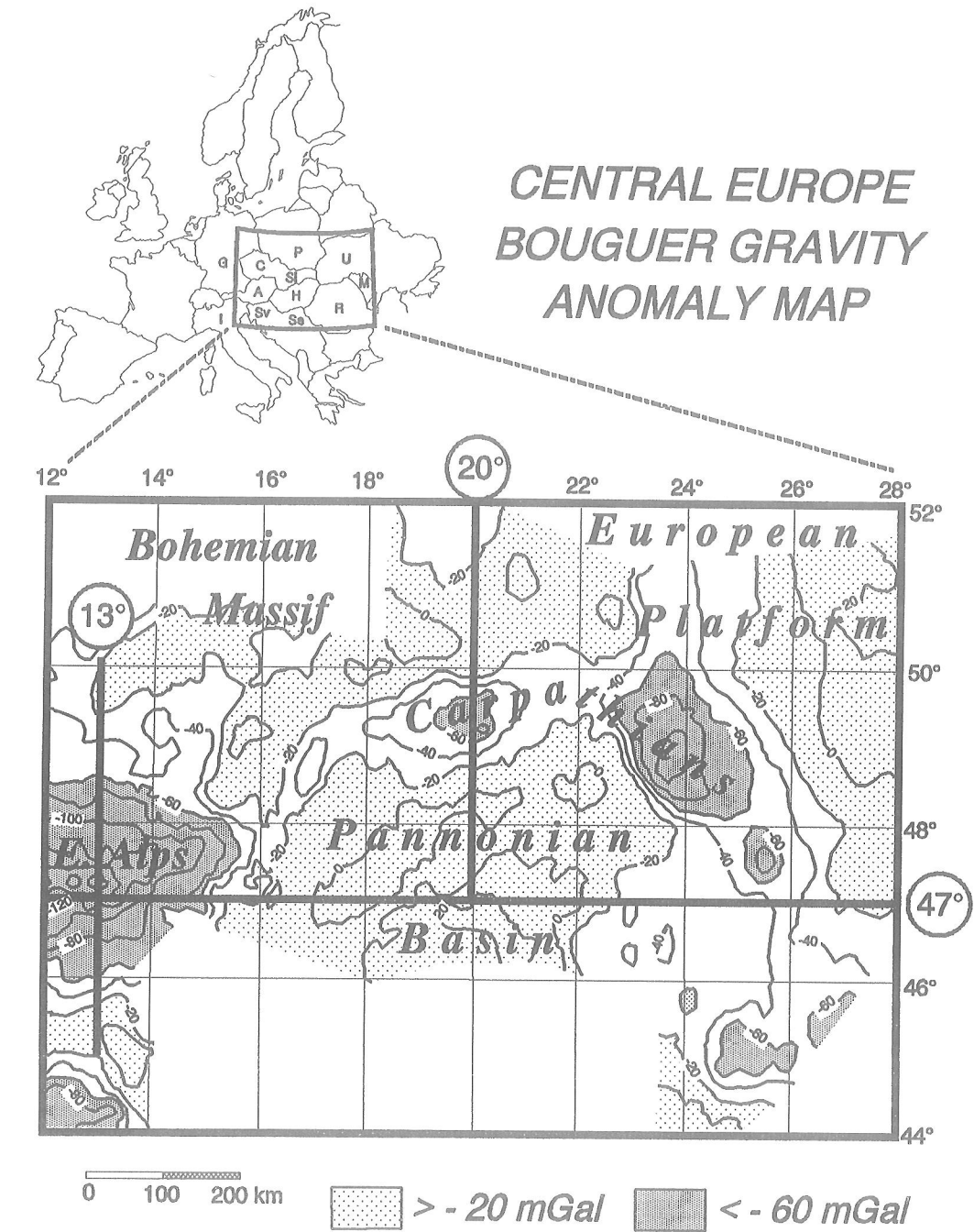


FIGURE 8.49 Bouguer gravity anomaly map of central Europe (Lillie et al., 1994). Gravity profiles along 13° E, 20° E, and 47° N shown in Figs. 8.50 and 8.51. Blank regions in southern and extreme northwestern and southeastern portions of map lacked sufficient station density to draw contours. A = Austria; C = Czech Republic; G = Germany; H = Hungary; I = Italy; M = Moldova; P = Poland; R = Romania; Se = Serbia; Sl = Slovakia; Sv = Slovenia; U = Ukraine.

CONTINENTAL COLLISION MODEL

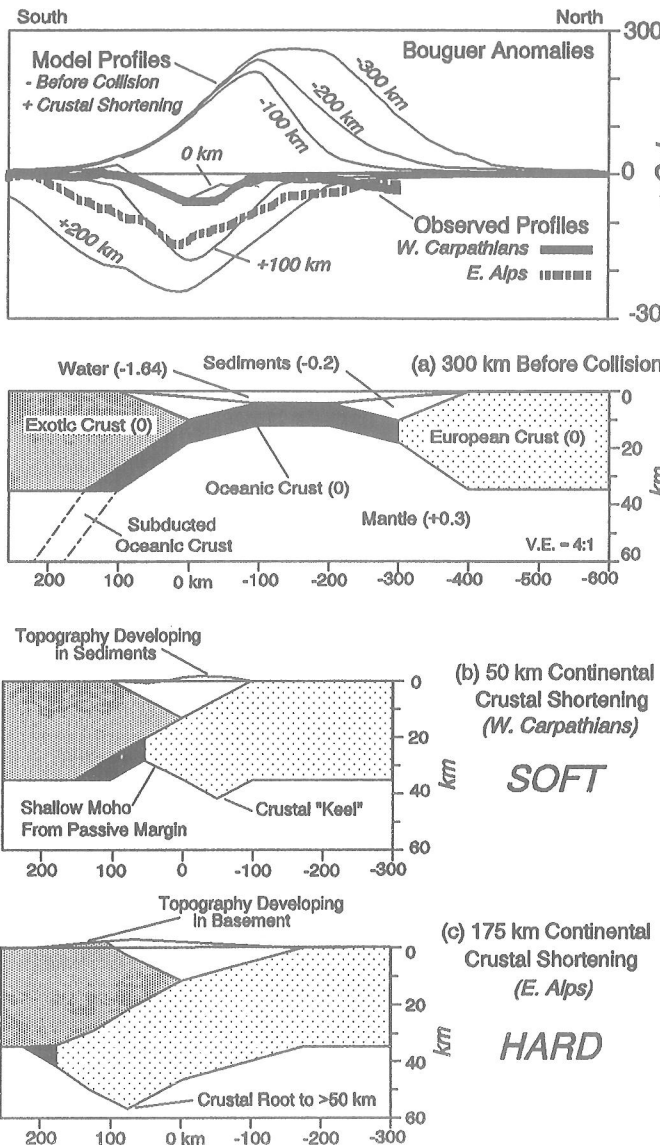


FIGURE 8.50 Balanced crustal model of ocean basin closure, maintaining local isostatic equilibrium (Lillie et al., 1994). The upper diagram shows the Bouguer gravity anomaly at different stages of continental collision. The -300 km profile represents the Bouguer anomaly when the ocean basin is 300 km wide; the 0 km profile shows the Bouguer anomaly when the continental crusts initially collide; the $+200$ km profile represents 200 of continued crustal convergence (shortening) after collision. Observed Bouguer anomaly profiles (Fig. 8.49) for the eastern Alps (13° E) and western Carpathians (20° E) are superimposed. a) Ocean basin and bordering passive and convergent margins, at a stage 300 km before the margins collide. Numbers in parentheses are density contrasts, in g/cm^3 . A Bouguer anomaly high occurs over the ocean basin (Fig. 8.34b). b) *Soft Collision*. Crustal configuration after one continent has overridden the edge of the other by 50 km, as in the western Carpathians. A narrow Bouguer anomaly low results from a depressed Moho ("keel") at the edge of the continental crust. c) *Hard Collision*. Situation after 175 km of continental crustal shortening (eastern Alps). A broad low results from a crustal root supporting the high topography of the mountains (Fig. 8.38b).

Mountain Range If a lithospheric plate supports the topographic load of a mountain range, effects of the load may be distributed over a broad region (Fig. 8.24b). Three important perturbations to gravity anomalies result (Fig. 8.52). 1) In the region of the load (mountains), the Moho is not depressed as much for the flexural case as it would be for the Airy case, resulting in higher gravity anomalies. Relative to the Airy model, flexural strength thus means that the region of the mountains is *undercompensated*. 2) In front of the mountains, there is a depression (foreland basin) where none existed in the Airy case. The top of the continental basement and Moho are depressed, leading to lower Bouguer gravity anomalies. Flexural strength thus means that the region of the foreland basin is *overcompensated*. 3) At the flexural bulges both the top of basement and the Moho are upwarped, resulting in free air and Bouguer gravity anomaly highs.

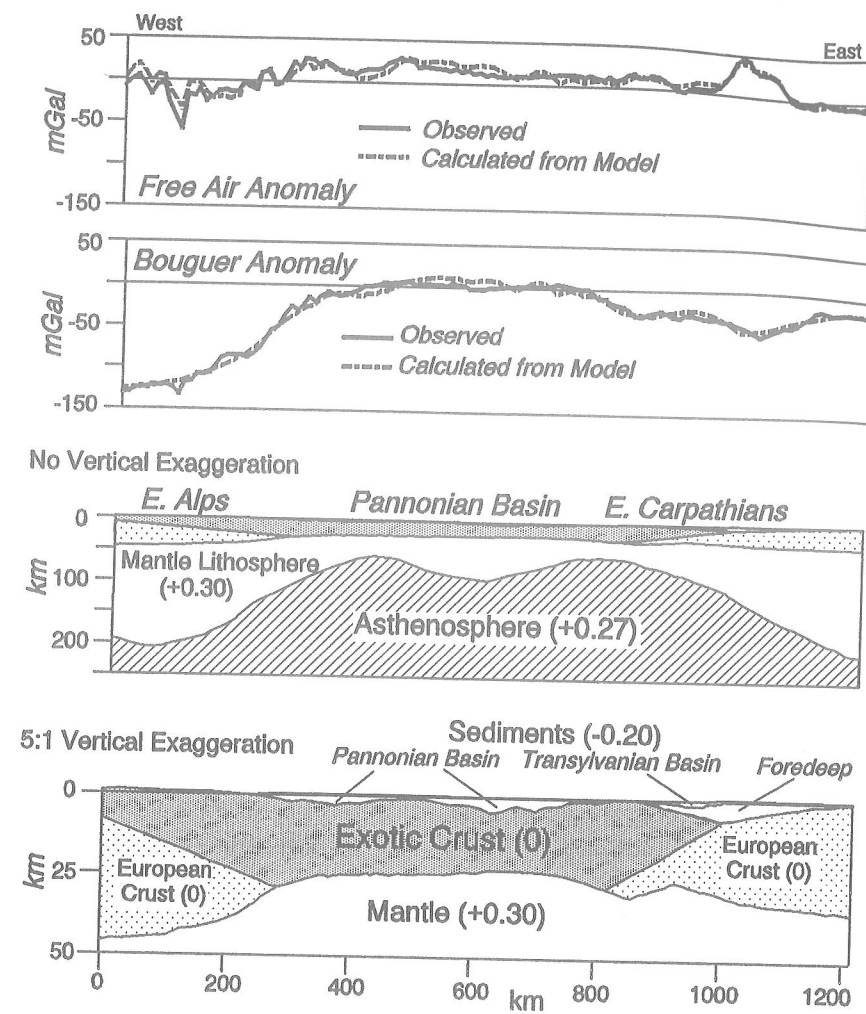


FIGURE 8.51 Observed free air and Bouguer gravity anomalies, along with anomalies computed from density model, from the Pannonian Basin in central Europe (47° N profile, Fig. 8.49). Assumed density contrasts (in g/cm^3) are relative to typical crustal materials. The model shows shallow mantle beneath thin crust, supported by elevated asthenosphere. Upper cross section shows entire model, down to 250 km depth, with no vertical exaggeration. Lower section is the upper 50 km of the model, at $5:1$ vertical exaggeration, illustrating the crustal thinning. The Bouguer anomaly high, in this case, reflects the shallow mantle. From Lillie et al. (1994).

Subduction Zone (Convergent Continental Margin) At a convergent continental margin, the main form of the free air anomaly is an edge effect similar to that of a passive continental margin (Fig. 8.33). In other words, the main contributions are a shallow, negative effect due to the water deepening seaward, compensated by the mantle shallowing in the same direction. Where the downgoing plate has flexural strength, loads from the overriding plate are distributed over a broad region (Fig. 8.24a). Analogous to the mountain range (Fig. 8.52), three things result. 1) Distributing the load means less depression of the Moho in the area of the accretionary wedge, enhancing the edge effect high. 2) The water deepens and the Moho is depressed in the region of the trench, enhancing the low portion of the edge effect on the free air anomaly. 3) The water and Moho are shallow at the flexural bulge, producing both free air and Bouguer gravity highs.

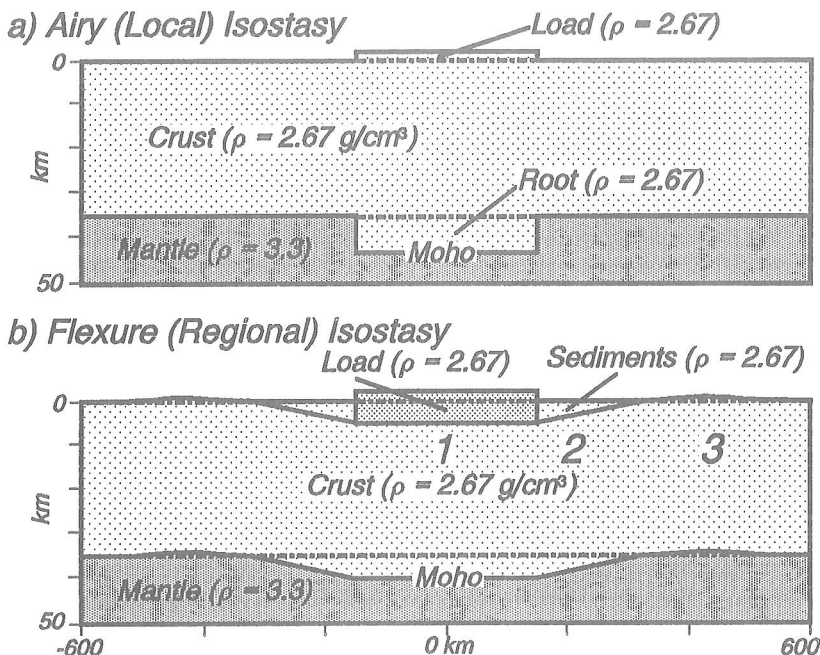
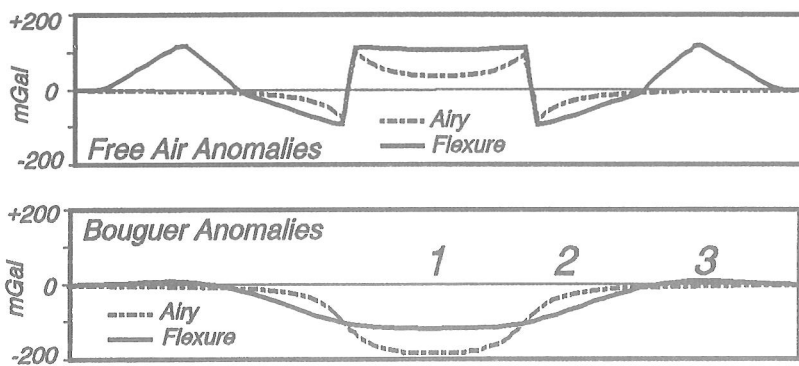


FIGURE 8.52 Hypothetical model showing free air and Bouguer gravity anomalies for a mountain range in local (Airy) and regional (flexure) isostatic equilibrium. a) Airy isostasy (Fig. 8.38) results in a free air anomaly profile with edge effects on both sides of the range, and values falling to near zero over the center. The Bouguer anomaly is the low due to the mountain root. b) Strength to the lithospheric plate results in higher gravity anomaly values over the range (1), with additional highs due to flexural bulging (3). Adjacent to the mountains (2), the downwarped Moho results in lower values compared to the Airy case; those values are even lower if there is significant density contrast between the sediments and crystalline crust.

The left portion of Fig. 8.39 shows this characteristic free air anomaly at the convergent continental margin of South America. The flexural bulge on the oceanic lithosphere results in a broad free air gravity high, adjacent to the edge-effect anomaly consisting of an enhanced low over the trench and a high over the continental edge. Similar high/low/high anomalies are evident at the Aleutian, Central American, and Caribbean subduction zones in the map on the back inside cover of this book.

EXERCISES

- 8-1 a) Using the equation for theoretical gravity, compute the difference in gravity expected at the equator compared to the poles.
- b) Draw sketches and compute the *relative contributions* (in mGal) for each of the three factors responsible for the difference (Fig. 8.4a). i) Use an equation for *centripetal acceleration* to estimate the negative contribution due to Earth's rotation.